

zkSTAR: A Zero Knowledge System for Time Series Attack Detection Enforcing Regulatory Compliance in Critical Infrastructure Networks

Paritosh Ramanan, H. M. Mohaimanul Islam, Abhiram Reddy Alugula

*School of Industrial Engineering and Management, Oklahoma State University
Stillwater, Oklahoma, USA*

{paritosh.ramanan, h_m_mohaimanul.islam, aalugul}@okstate.edu

Abstract—Industrial control systems (ICS) form the operational backbone of critical infrastructure networks (CIN) such as power grids, water supply systems, and gas pipelines. As cyber threats to these systems escalate, regulatory agencies are imposing stricter compliance requirements to ensure system-wide security and reliability. A central challenge, however, is enabling regulators to verify the effectiveness of detection mechanisms without requiring utilities to disclose sensitive operational data. In this paper, we introduce zkSTAR, a cyberattack detection framework that leverages zk-SNARKs to reconcile these requirements and enable provable detection guarantees while preserving data confidentiality. Our approach builds on established residual-based statistical hypothesis testing methods applied to state-space detection models. Specifically, we design a two-pronged zk-SNARK architecture that enforces (i) temporal consistency of the state-space dynamics and (ii) statistical consistency of the detection tests, enabling regulators to verify correctness and prevent suppression of alarms without visibility into utility-level data. We formally analyze the soundness and zero-knowledge properties of our framework and validate its practical feasibility through computational experiments on real-world ICS datasets. As a result, our work demonstrates a scalable, privacy-preserving alternative for regulatory compliance for ICS driven critical infrastructure networks.

Index Terms—Zero Knowledge Proof, Industrial Control Systems, Data-driven attacks, Regulatory Compliance.

1. Introduction

The convergence of information and operational technologies (IT–OT) through widespread IoT adoption has expanded the attack surface for data-driven cyber intrusions. Such attacks often target industrial control systems (ICSs), degrading asset performance and triggering cascading failures across critical infrastructure networks (CINs). While detection occurs locally at utilities, regulatory bodies such as Information Sharing and Analysis Centers (ISACs) aggregate alarms in real time to enhance situational awareness and reduce false positives [1]. The effectiveness of these regulators, however, hinges on the integrity and reliability of local detection data. Recent real-world incidents [2]–[4] have demonstrated that adversaries can compromise both

IT and OT layers to obscure, delay, or disable detection of underlying anomalies. Such incidents expose a fundamental regulatory blind spot pertaining to verifying the integrity of reported detections without re-auditing raw operational data. Moreover, inconsistent or low-quality local insights can undermine the ISAC’s ability to construct a reliable network-wide situational awareness model, potentially causing unnecessary service disruptions [1]. To address this gap, we introduce zkSTAR, a framework enabling publicly verifiable detection of data-driven ICS attacks in complete zero knowledge of local ICS state-space dynamics.

zkSTAR addresses a critical regulatory gap by enabling provable temporal and statistical consistency verification of ICS detections. Leveraging knowledge-soundness and provably consistent outcomes, it ensures that compromised utilities cannot falsify or suppress alarms even if their IT–OT stacks are breached. The framework enables verifiable regulatory oversight while preserving utility data confidentiality [1], eliminating the need for costly, privacy-intrusive audits that have long impeded secure information sharing [5]. Additionally, by adopting an on-demand, lazy proof generation paradigm, zkSTAR ensures a low utility overhead as well.

Conventional ICS anomaly detection relies on state-space models that estimate expected sensor behavior and compute residuals to flag deviations from steady-state conditions [6]. Statistical hypothesis tests on these residuals distinguish normal from abnormal operation, triggering alarms when observed measurements significantly diverge from model predictions [7]. With existing approaches, regulators can verify such detection outcomes only through full data audits of ICS operations—requiring utilities to relinquish proprietary IoT datasets and raising severe privacy and data-governance concerns. Moreover, utilities must demonstrate both temporal consistency wherein successive state estimates are derived from prior ones; and statistical consistency in which alarms follow valid hypothesis test procedures. These audits are costly, slow, and incompatible with real-time oversight.

To overcome these limitations, zkSTAR delivers provable temporal and statistical consistency guarantees for state space driven statistical detection of data driven ICS attacks. At its core, zkSTAR is specifically designed to validate consistency claims for ICS systems with highly non-linear state space dynamics in complete zero knowledge. zkSTAR

is based on the zkSNARK (zero-knowledge succinct, non-interactive argument of knowledge) paradigm providing publicly verifiable attack detection outcomes for a state space modeling paradigm in a trustworthy fashion. zkSTAR operates in an on-demand compliance mode, where regulators issue proof-generation requests to utilities whenever verification of local detections is required. We present a detailed overview of our contributions as follows:

- We develop a zkSNARK based prediction framework that leverages an extended Kalman filter based model to detect data driven attacks on ICSs of utility stakeholders in complete zero-knowledge of local sensor or state space dynamics.
- We establish formal security guarantees for zkSNARK driven regulatory compliance with temporal and statistical consistency proofs of detection outcomes that also ensure resistance to attack-suppression under knowledge soundness property.
- We design a zkSNARK based kernel decomposition scheme that provides the ability to prove temporal and statistical consistency claims in a scalable and computationally efficient manner.
- We detail the performance of zkSTAR with respect to detailed case studies involving real-world datasets using a REST-API driven container-based computational testbed.

Overall, we show that zkSTAR enforces integrity of detection proofs under adversarial falsification, preventing utilities from reusing stale states or forging alarms—making it a security enforcement layer for regulatory trust.

2. Related Works

Attacks on industrial control systems (ICSs) that target IT layers can often be detected through network traffic monitoring [8], [9]. However, data-driven attacks that manipulate sensor or control data can evade such approaches by simultaneously impacting both IT and OT layers [10]–[12], potentially causing cascading failures across critical infrastructure. More recently, there have been several attack vulnerabilities that have been discovered such as like Industroyer and Industroyer2 [4], Triton [3] and Stuxnet [2]. These vulnerabilities have demonstrated the feasibility of joint manipulation of control systems and monitoring data which have motivated the need for robust verifiable detection mechanisms for ICS.

To address some of these challenges, several *model-based* mechanisms have been proposed [13]–[15]. Among these, *Kalman filter based* approaches are particularly robust and flexible [6], [7], [16]–[18], leveraging residuals from state-space models as statistical evidence for anomaly detection. These residual-based tests differentiate routine faults from malicious attacks [16] and can support decentralized, network-wide alarm dissemination [17].

From the compliance perspective, however, it is essential for the regulator to receive timely notifications regarding attack detection at utility stakeholders in addition to verifying the integrity of attack detection so as to limit its

network-wide impacts and reduce false alarm rates [1], [17]. Therefore, regulatory compliance goals would ideally enable stakeholders to provide publicly verifiable detection outcomes that are accurate and trustworthy without exposing private operational data. Achieving such verifiable compliance under privacy constraints motivates the use of zero-knowledge proofs [19], enabling a prover to convince a verifier of correctness without revealing sensitive information.

Originating from foundational work by Goldwasser *et al.* [20] and Blum *et al.* [21], zero-knowledge proofs evolved into succinct, non-interactive forms (zk-SNARKs) that support efficient verification [22]–[28]. Recent applications in machine learning verify training integrity and model ownership [29]–[32]. While existing zk-SNARK frameworks enable general-purpose verifiable computation, none target the verification of dynamical system integrity or hypothesis-test correctness which are cornerstones of industrial attack detection. Recent works on verifiable differential privacy [19] and secure multiparty analytics [33] focus primarily on data confidentiality but not on verifiable detection correctness, a gap zkSTAR directly addresses. To alleviate this core critical gap, this paper introduces zkSTAR, a framework that enables provable, privacy-preserving verification of Kalman filter-based detection mechanisms, paving the way for regulatory compliance in CINs.

3. Nonlinear State Space Modeling

For developing zkSTAR, we leverage the extended Kalman Filter (EKF) state space models owing to their flexibility in handling highly non-linear spatial and temporal interdependencies among several ICS components [34]. Therefore, we characterize the EKF-based, utility-level attack detection model as a foundational component of zkSTAR for achieving regulatory compliance under zero knowledge. Within zkSTAR, we develop a state-space formulation capable of identifying attack-induced anomalies through locally executed statistical hypothesis tests.

3.1. Extended Kalman Filter Model

We present a brief overview of the EKF model in this section while a detailed description of the model has been provided in Appendix A.1. Let g, h denote the state transition and observation functions respectively, $x_t \in R^m$ represents the latent space embedding, $u_t \in R^m$ represents the control action and $y_t \in R^d$ represents noisy sensor measurements from asset sensors. Additionally, let process and measurement noises follow multivariate normal distributions $N(0, Q_t)$ and $N(0, R_t)$ respectively. Now, we define our

EKF model based on the following equations:

$$\hat{x}_{t|t-1} = g(\hat{x}_{t-1|t-1}, u_{t-1}), \quad (1)$$

$$r_t = y_t - h(\hat{x}_{t|t-1}), \quad (2)$$

$$P_{t|t-1} = G_t P_{t|t-1} G_t^T + Q_{t-1}, \quad (3)$$

$$S_t = (H_t P_{t|t-1} H_t^T + R_t), \quad (4)$$

$$K_t = P_{t|t-1} H_t^T S_t^{-1} \quad (5)$$

$$\hat{x}_{t|t} = \hat{x}_{t|t-1} + K_t r_t \quad (6)$$

$$P_{t|t} = (I - K_t H_t) P_{t|t-1} \quad (7)$$

In our EKF model, we have $P_{t|t-1}, P_{t|t}$ represent the predicted and the updated covariance estimates respectively, while S_t represents the residual covariance at t . The state transition and the observation matrices at t given by G_t, H_t respectively are computed using the Jacobians of g, h .

3.2. Hypothesis Test for Anomaly Detection

We consider residual covariance $S_t = U_t \Sigma_t U_t^T$ coupled with residual measurements r_t for detecting covert data-driven attacks [6]. Without loss of generality we note that it is also possible to apply our techniques for detecting false data injection by monitoring R_t . We denote the standardized vector of PC scores as $\tau_t = (S_t)^{-1/2}(r_t) = U_t \Sigma_t^{-1/2}(r_t)$ such that $\tau_t \sim N(0, I)$ [6], [35]. This implies that $\|\tau_t\|_2^2 \sim \chi_p^2$, where $p < d$ is the degrees of freedom corresponding to the number of principal components used [35].

$$\rho = \begin{cases} 1, & \text{if } T_{\chi^2, t} = \|\tau_t\|_2^2 > \chi_{m, \alpha}^2, \\ 0, & \text{otherwise.} \end{cases} \quad (8)$$

A generic hypothesis testing procedure applicable to sensor and residual monitoring has been discussed in greater detail in [16]. We define a measure of *probabilistic similarity* to help establish the distinctness of two sensor measurement vectors as stated in Definition 1.

Definition 1 (Probabilistic Similarity). *Two distinct \tilde{y}_{t+1}, y_{t+1} with corresponding test statistics $\tilde{T}_t = \text{ChiTestStat}(\tilde{y}_{t+1}; \alpha, m)$ and $T_t = \text{ChiTestStat}(y_{t+1}; \alpha, m)$ are deemed to be probabilistically similar if $\tilde{T}_t > \chi_{p, \alpha}^2$ and $\tilde{T}_t > \chi_{p, \alpha}^2$.*

The concept of probabilistic similarity is particularly useful while handling issues for numerical precision issues wherein the sensor data measurement stored and processed in the ICS differs from the original value recorded by the sensors. We now proceed towards theoretical characterization of the zkSNARKs to enforce temporal and statistically consistent detection outcomes.

4. Regulatory Compliance using zkSNARKs

Detecting attacks requires monitoring covariance matrices of the residuals to drive the underlying χ^2 hypothesis tests. However, publicly validating alarms by an external entity such as a regulator would require the disclosure of residual vectors and covariance matrices that enable these hypothesis tests. Therefore, a critical regulatory challenge is the verification of the hypothesis test outcomes as reported

by the utilities in the absence of their state space residual and covariance estimates. Zero-knowledge proofs form a viable alternative for solving these critical pain points by helping achieve public verification of utility level attack detection outcomes for regulatory purposes. Therefore, in this paper, we employ zero knowledge proofs to enable regulatory compliance and verification. We concentrate on a utility-oriented subsystem represented by a state-space model as outlined in Section 3 that is meant to be captured in a zkSNARK framework. As a result, our methodology specifically leverages zk-SNARKs to assert temporal consistency and statistical consistency for utility-level χ^2 hypothesis tests in zero-knowledge of local state space dynamics.

4.1. Zero Knowledge Preliminaries

We begin our discussion of zk-SNARK based regulatory compliance schemes for cyber attack detection by establishing four fundamental definitions.

Definition 2 (Hash Function). *A hash function denoted by hash can be defined such that it can consume arbitrary length inputs so as to map to fixed length outputs of size n*

$$\text{hash} : \{0, 1\}^* \rightarrow \{0, 1\}^n$$

Definition 2 portrays a hashing function that will be utilized to ensure the integrity of state space estimates. We assume that the function hash preserves integrity, one-wayness, hiding and collision resistance properties [36].

Definition 3 (Pretrained State Space Model). *The non-linear Kalman Filter based state space can be represented by a pretrained model \mathcal{M} parametrized by θ such that the following conditions hold*

$$\begin{aligned} \mathcal{M}(\Delta_t^{in}; \theta) &\mapsto \Delta_t^{out} \\ \Delta_t^{in} &= (\mathcal{H}_t^{in}, \hat{x}_{t|t}, y_t) \\ \Delta_t^{out} &= (\mathcal{H}_t^{out}, \rho_t, \hat{x}_{t+1|t+1}, r_t, K_t, Q_t, R_t) \\ \mathcal{H}_t^{in} &= \text{hash}(\hat{x}_{t|t}), \text{ and } \mathcal{H}_t^{out} = \text{hash}(\hat{x}_{t+1|t+1}) \end{aligned}$$

Definition 3 helps define a pretrained LSTM based model which encapsulates the non-linear Kalman Filter based state space as defined in Equations (1)-(7). More specifically, the inputs and outputs of \mathcal{M} at time t are represented by Δ_t^{in} and Δ_t^{out} respectively.

Definition 4 (zk-SNARK Setup Phase). *Given a standard security parameter λ , the zk-SNARK setup phase can be defined by function Setup such that*

$$\text{Setup}(1^\lambda, \mathcal{M}, \theta) \mapsto (pk, vk)$$

Definition 4 discusses the setup phase of the zk-SNARK proof mechanism that involves the generation of pk and vk that represent the proving and verification keys respectively. We assume that the setup phase needs to be executed once for each utility. Such assumptions are driven by the fact that a pretrained, high accuracy state-space model \mathcal{M} does not require frequent updates to the weight parameter. However,

we note that the setup function needs to be re-evaluated upon each update of the weight parameter θ .

Definition 5 (zk-SNARK Proving Phase). *The zk-SNARK proving phase is defined by function Prove such that*

$$\text{Prove}(pk, \theta, \mathcal{M}, \Delta_t^{in}, \Delta_t^{out}) \mapsto \Pi_t$$

Definition 5 details the proving phase of the zk-SNARK. The Prove function consumes the proving key pk , \mathcal{M} parametrized by θ as well as the inputs Δ_t^{in} and outputs Δ_t^{out} at time t to generate a proof artifact Π_t . The Prove function is executed for each timestep t at the utility level.

Definition 6 (zk-SNARK Verification Phase). *The verification of zk-SNARK proof artifacts can be represented by the function Verify such that*

$$\text{Verify}(vk, \Pi_t, \Delta_t^{in}, \Delta_t^{out}) \mapsto \Phi_t$$

Definition 6 presents the Verify function that aims to enable regulators to verify reported proofs Π_t based on the verification key vk as well as inputs Δ_t^{in} and Δ_t^{out} . The Verify function provides output $\Phi_t \in \{0, 1\}$ which is indicative of successful verification.

Zero knowledge regulatory compliance for attack detection relies on two fundamental operational attributes of temporal and statistical consistency. We argue that these two fundamental operational attributes are necessary and sufficient conditions to enable zero-knowledge regulatory compliance verification. Our argument is based on the ability of the pretrained model \mathcal{M} to recursively ensure that state space estimates are derived from previous predictions while being statistically consistent with expected residual covariance. In the following subsections, we formally state each operational attribute separately as a precursor for guaranteeing integrity of detection outcomes.

4.2. Temporal Consistency

Temporal consistency (TC) pertains to the recursive relationship between *a posteriori* state space estimates at t and $t + 1$ respectively. Temporal consistency constraint encoded in the non-linear Kalman filter model ensures that the posteriori estimate $\hat{x}_{t+1|t+1}$ is a derivative of $\hat{x}_{t|t}$. We state this formally as part of Definition 7.

Definition 7 (Temporal Consistency). *The state space system is considered to be temporally consistent if for each consecutive time step pairs $t, t + 1$, the following holds.*

$$x_t^{out} = x_{t+1}^{in}$$

where,

$$x_t^{out} = \hat{x}_{t|t-1} + K_t r_t, \text{ and, } \hat{x}_{t+1|t} = g(x_{t+1}^{in}, u_t)$$

As a consequence of Definition 7 we can make the temporal consistency claim presented in Theorem 4.1.

Theorem 4.1 (zk-STAN TC Conditions). *Given every consecutive time step pairs $t, t + 1$ such that $vk_t = vk_{t+1}$,*

$pk_t = pk_{t+1}$, temporal consistency can be asserted if and only if the following conditions hold

$$\mathcal{H}_{t+1}^{in} = \mathcal{H}_t^{out}, \text{ and } \Phi_{t+1} = 1$$

Proof. Proof provided in Appendix B.1 \square

Theorem 4.1 shows that the integrity of temporal posteriori predictions from an EKF driven state space system can be established using a zkSNARK proof artifact if and only if the verification keys remain invariant; the hash commitments of the inputs to the EKF model at each time step is equal to that of the previous EKF output; and the proof artifact itself can be verified using the verification keys. In other words, Theorem 4.1 demonstrates that if temporally inconsistent values are used for carrying out the EKF predictions, then either the verification fails for at least one time step or the keys used for verifying the proof artifact will differ. Therefore, to establish temporal consistency from a regulatory perspective, it is necessary and sufficient to check for the invariance of keys, alignment of hash commitments and the verification status across successive time steps.

4.3. Statistical Consistency

We consider the local attack detection framework characterized by the χ^2 hypothesis test presented in Section 3.2. The χ^2 test relies on the residual and state space estimates provided by \mathcal{M} that is parametrized by θ . As a result of Equation (8), the local attack detection framework is expected to yield an alarm value denoted by $\rho_t = 1$, when an attack is taking place while maintaining $\rho_t = 0$ under normal circumstances. We utilize these fundamental principles to establish the notion of statistical consistency (SC). For the purposes of statistical consistency, we denote the genuine and the reported outcomes of the χ^2 test as $\rho_t^{real} \in \{0, 1\}$ and $\rho_t^{rep} \in \{0, 1\}$ respectively.

Definition 8 (Statistical Consistency). *The local attack detection framework is deemed to be statistically consistent if $\rho_t^{real} = \rho_t^{rep}$.*

Statistical consistency ensures that reported alarm values are consistent with the outcomes of the attack detection frameworks that is based on the χ^2 hypothesis test. However, from a real-world deployment perspective, the sensor data measurements observed in the field might have slight inaccuracies as they are transmitted across the utility ICS. These inaccuracies could arise due to sensor calibration errors and numerical precision limitations especially on inexpensive sensor hardware which are commonly found in large scale ICS. In such cases, expecting to acquire and store a copy of the sensor data measurement at different levels of the ICS that is numerically identical to the one that was originally recorded by the sensor is unrealistic. However, given the inherent robustness of hypothesis tests, utilizing a sensor measurements that is similar but not necessarily identical to the originally recorded value is sufficient for establishing statistical consistency. As a result, we develop Lemma 1 as a means to formally establish the notion of probabilistic

similarity of sensor measurements and its connection to statistical consistency of the zkSTAR framework.

Lemma 1. *Probabilistically similar sensor measurement realizations \tilde{y}_t, y_t are necessary and sufficient conditions for observing statistically consistent outcomes $\tilde{\rho}_t, \rho_t$.*

Proof. Proof provided in Appendix B.2 \square

Lemma 1 shows that as long as the sensor signal used to carry out EKF predictions is probabilistically similar to the true value of the sensor signal the zkSTAR framework will continue to deliver statistically consistent alarm detection outcomes. Moreover, with the help of Lemma 1, we can also state that a data driven ICS attack orchestration might in theory go undetected under the zkSTAR framework when the malicious sensor measurements are probabilistically similar to the originally recorded sensor measurements. Practically, such attacks end up being inconsequential [16] since they are unable to effect any material damage to the ICS assets. Therefore, Lemma 1 serves as the basis for Theorem 4.2 which derives an integral link between key invariance, statistical and temporally consistency.

Theorem 4.2 (zk-SNARK SC Conditions). *Given consecutive time step pairs $t, t + 1$ with (vk_t, pk_t) and (vk_{t+1}, pk_{t+1}) , temporal consistency implies statistical consistency.*

Proof. Proof provided in Appendix B.3 \square

Theorem 4.2 shows that alarm values obtained from zkSTAR can be deemed statistically consistent if they share the same proving and verification keys and if TC conditions are met according to 4.1. As a result, a regulatory agency can deem reported alarms from utility stakeholder as a violation of SC claims despite successful verification if conditions pertaining to key-invariance or temporal consistency are not met. We formalize the security model with the help of Theorems 4.1 and 4.2 in the subsequent section.

4.4. Security Model and Guarantees

We prove that zkSTAR satisfies knowledge-soundness, guaranteeing that any attempt to forge or reuse stale state estimates for regulatory verification violates the TC-SC consistency relation, thereby ensuring attack-suppression detection. For a given timestep t , we denote Ω_t to be the witness for corresponding the state space model \mathcal{M} parametrized by θ . Using Theorems 4.1 and 4.2, the temporal-statistical consistency relation \mathcal{R}_t can be defined as in Equation (9) from the perspective of a non-attack.

$$\begin{aligned} \mathcal{R}_t[(\Delta_t^{in}, \Delta_t^{out}), \Omega_t] = & [(\mathcal{M}(\Delta_t^{in}; \theta) = \Delta_t^{out}) \\ & \wedge (\mathcal{H}_{t+1}^{in} = \mathcal{H}_t^{out}) \wedge (T_{\chi^2, t}(\tau_t) \leq \chi^2_{m, \alpha})]. \end{aligned} \quad (9)$$

We consider a utility prover \mathcal{U} undergoing a data-driven cyberattack starting at timestep $t^{attack} \gg t^{init}$ where t^{init} represents the initial time step pertaining to the setup phase (Definition 3). For concreteness, we base our analysis on the Halo2 backend for establishing knowledge-soundness.

For the analysis of the security model and to establish knowledge-soundness, we assume that the objective of the malicious attacker is to carry out the attack while suppressing attack detection. Moreover, we assume that the compromised utility possesses an extractor $\mathcal{E}^{\mathcal{U}}$ that produces a valid proof Π_t which results in $\Phi_t = 1$ with an incorrect witness $\mathcal{E}^{\mathcal{U}}(\Delta_t^{in}, \Delta_t^{out}) \neq \Omega_t$, with a non-negligible probability. Formally, we define attack suppression using Definition 9.

Definition 9 (Detection Suppression). *The detection framework characterized by $\mathcal{M}(\cdot; \theta)$ is deemed to have been suppressed when the following conditions hold*

$$\begin{aligned} \text{Verify}(vk_t, \Pi_t, \Delta_t^{in}, \Delta_t^{out}) &= 1 \\ ((\Delta_t^{in}, \Delta_t^{out}), \mathcal{E}^{\mathcal{U}}(\Delta_t^{in}, \Delta_t^{out})) &\notin \mathcal{R}_t \end{aligned}$$

As a result using the TC and SC claims detailed in Theorems 4.1 and 4.2, we characterize the infeasibility of detection suppression in Theorem 4.3.

Theorem 4.3 (Detection Suppression and Knowledge Soundness). *Given a utility prover \mathcal{U} a timestep $t > t^{attack}$, detection suppression occurs with only negligible probability under the knowledge-soundness property of the underlying proving system. Furthermore, infeasibility of detection suppression is equivalent to violation of either proof verification or of the temporal-statistical consistency relation \mathcal{R}_t .*

Proof. Proof provided in Appendix B.4. \square

Theorem 4.3 fundamentally demonstrates that a utility undergoing an attack must either fail proof verification or violate TC-SC relations enforced by zkSTAR. In other words, an under-attack utility cannot fabricate or reuse stale system states without detection, since any such attempt would contradict the knowledge-soundness of the Halo2 backend rendering attack suppression cryptographically infeasible.

5. Computational Architecture of zkSTAR

The zkSTAR architecture is based on the existence of two components comprising the utility as the prover and the regulator as the verifier. As a result, the algorithmic core of zkSTAR focuses on the utility component, encapsulating the utility level EKF model discussed in Section 3 in a zero-knowledge framework. The regulatory component deals with verifying the utility generated proof artifacts and asserting TC, SC and detection suppression claims of utilities.

The framework is designed to generate proofs in an *on-demand, lazy fashion* using keys generated at the utilities. As a result, utilities commit to the EKF model a priori and use the keys to generate only witnesses in real time containing state space estimates including residuals, covariances and test statistics for each detection window. A regulator can invoke proof generation on-demand at the utility level for specific detection windows as per verification needs.

When attempting to encapsulate the utility level EKF model into a zkSNARK structure, we face three crucial challenges. First, asserting temporal consistency is challenging due to the highly non-linear and dynamic nature of utility

based ICS subsystems. Second, ensuring statistically consistent detection outcomes without revealing parameters of the statistical test is difficult. Lastly, high-fidelity streaming sensor datasets possess a fine temporal granularity that leads to an additional layer of computational complexity when characterizing attacks. In order to address these challenges, the zkSTAR framework adopts a temporal decomposition scheme that specifically caters to TC and SC aspects.

5.1. Temporal Decomposition Scheme

We consider a real-time attack detection horizon that is discretized into a sequence of detection windows denoted by set $\mathcal{W}_i, \forall i \in \{1, 2, \dots\}$. Each detection window \mathcal{W}_i is in turn divided into a set of W TC intervals. Each TC interval is represented by $w_{ij}, \forall j \in \{1, W\}$ and is primarily geared towards enforcing TC across multiple prediction time steps. Every TC interval consists of D consecutive timestamps such that $w_{ij} = \{t_{w_{ij}}, t_{w_{ij}} + 1, t_{w_{ij}} + 2 \dots t_{w_{ij}} + D\}$, where $t_{w_{ij}}$ is the starting timestamp of TC interval w_{ij} . The relationship between each detection window \mathcal{W}_i , its constituent TC intervals w_{ij} and corresponding timesteps can be compactly denoted using Equations (10) and (11).

$$\mathcal{W}_i = \{w_{i1}, w_{i2}, \dots w_{iW}\}, \forall i \in 1, 2, \dots \quad (10)$$

$$w_{ij} = \{t_{w_{ij}}, t_{w_{ij}} + 1, t_{w_{ij}} + 2 \dots t_{w_{ij}} + D\}, \forall j \in \{1, W\} \quad (11)$$

Without loss of generality, let us consider a detection window \mathcal{W} and its constituent TC intervals $w_j \in \mathcal{W}, j \in \{1, W\}$. We know from Section 3 that for any time step $t_w + k \in w, r_{t_w+k} \sim N(0, S_{t_w+k})$ where r_{t_w+k}, S_{t_w+k} are the residual and the covariance matrix predicted by the pre-trained EKF model for time step $t_w + k$. Since $r_{t_w+k} \sim N(0, S_{t_w+k})$, the residuals and covariance matrices can be aggregated across all TC intervals in a detection window to yield r_W and S_W denoted in Equation (12).

$$r_W = \sum_{j=1}^W \sum_{k=1}^D r_{t_{w_j}+k}, S_W = \sum_{j=1}^W \sum_{k=1}^D S_{t_{w_j}+k} \quad (12)$$

As a result of hierarchical decomposition, there exists a distinct detection alarm ρ_W for each detection window \mathcal{W} .

The temporal decomposition scheme paves the way for zkSNARKs to help enforce integrity of state space predictions based on a pre-committed EKF model. However, the zkSNARK circuit size grows exponentially with the growth in the detection window size making the proof generation step computationally expensive especially for larger systems. Therefore, in order to balance practicality and computational efficiency, we adopt a kernel based strategy that decomposes various compute tasks pertaining to an EKF model. Specifically, we design zkSNARK based kernels that target individual sub tasks pertaining to TC and SC attributes of EKF predictions and detection outcomes capable of operating on batched EKF residual outputs. We note that current zkSNARK frameworks such as `ezkl` lack support for linear solvers, SVD decompositions, and derivative evaluations of complex sub modules due to their high computational cost in zero knowledge [37]. To address

these limitations, we employ a *compute-offline-validate-online* strategy, performing such expensive operations off-circuit while verifying their consistency with the state-space model within the zkSNARK circuit.

5.2. zkSNARK based Temporal Kernels

For ensuring temporally consistent outcomes, our kernel design strategy involves breaking down distinct components of the EKF model inference. Specifically, we decompose the EKF inference over a single TC interval into distinct phases that pertain to validating the consistency of the Kalman gain matrix with the state covariance and process and measurement Jacobians; inference of the pre-committed EKF model on one timestamp of the TC interval; and accumulating the residual and its covariance sum across the entire TC interval.

Kalman Reconstruction Check (KRC) Kernel: The EKF model presented in Section 3 relies on successive linear solves of Equation (5) in order to determine the Kalman gain K_t . However, this poses a major challenge since implementing linear system solvers within a zkSNARK is computationally very expensive. Therefore, we develop a computational kernel tailored for the zkSNARK paradigm that demonstrates that offline computed matrices Kalman gain K , LSTM Jacobian H , residual covariance S and state covariance P are consistent with respect to the state space EKF model. The result is the KRC kernel depicted in Algorithm 1 which yields a boolean output κ_t depending on whether the error in Equation (5) is below or above ϵ_{KC}

Algorithm 1 zkSTAR Kernel for Kalman Gain Reconstruction

```

1: function KRC-KERNEL( $K, S, H, P, \epsilon$ )
2:    $\kappa \leftarrow 0$ 
3:   if  $\|KS - PH^\top\|_2^2 < \epsilon$  then  $\kappa \leftarrow 1$ 
4:   end if
5:   return  $\kappa$ 
6: end function

```

Extended Kalman Filter (EKF) Kernel: For enforcing the state space dynamics at each timestamp in zero knowledge, we develop a dedicated zkSNARK based computational kernel for EKF denoted by \mathcal{M}_t^{EKF} .

$$\mathcal{M}^{EKF} : \underbrace{\mathcal{I}_t^{EKF} = \{\mathcal{X}_{t-1}, y_t, \mathcal{J}_t\}}_{\text{EKF input at timestamp } t} \mapsto \underbrace{\mathcal{O}_t^{EKF} = \{r_t, S_t, \kappa_t\}}_{\text{EKF output at timestamp } t} \quad (13)$$

Fundamentally, \mathcal{M}^{EKF} forms a mapping between input tuple \mathcal{I}_t^{EKF} and output tuple \mathcal{O}_t^{EKF} . The input tuple in turn consists of $\mathcal{X}_{t-1} = \{x_{t-1|t-1}, P_{t-1|t-1}\}$ which denotes a collection of state and covariance estimates from the prior time step. $\mathcal{J}_t = \{G_t, H_t, K_t\}$ represents a collection of the Jacobian matrices of the LSTM and feed-forward neural layers in the EKF formulation along with the Kalman gain matrix that are computed offline. Lastly, y_t represents the sensor data sampled at time stamp t . The output tuple \mathcal{O}_t^{EKF} consists of r_t, S_t, κ_t , which denote the residual and its

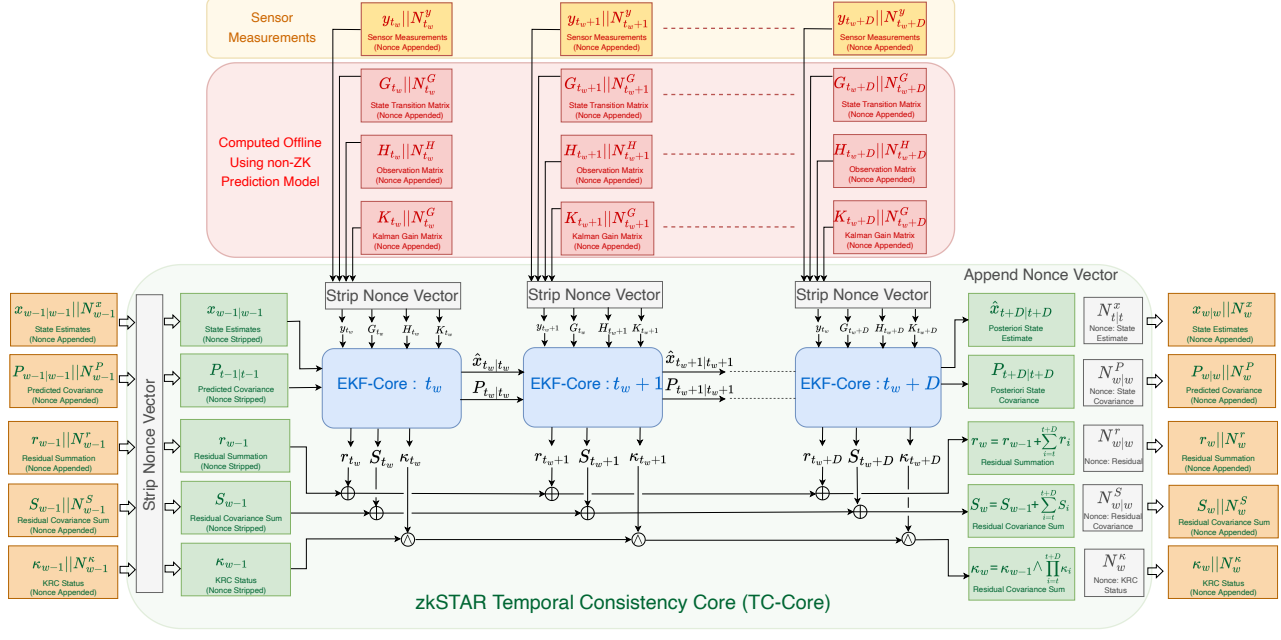


Figure 1: Temporal consistency handling in zkSTAR

Algorithm 2 zkSTAR Kernel for Extended Kalman Filter

```

1: function EKF-KERNEL( $x_{t-1|t-1}, P_{t-1|t-1}, y_t, G_t, H_t, K_t$ )
2:   compute  $\hat{x}_{t|t-1}$  using Equation (1).
3:   compute  $r_t$  using Equation (2)
4:   compute priori covariance  $P_{t|t-1}$  using Equation (3)
5:   compute innovation  $S_t$  using Equation (4).
6:    $\kappa_{t_w} \leftarrow \text{KRCKERNEL}(K_t, S_t, H_t, P_{t|t}, \epsilon_{KC})$ 
7:   update posteriori estimate  $\hat{x}_{t|t}$  using Equation (6)
8:   update the state posteriori covariance  $P_{t|t}$  using (7)
  return  $r_t, S_t, \kappa_t$ 
9: end function

```

covariance as well as the status of the Kalman Gain reconstruction check. Algorithm 2 represents the computational kernel for EKF within the zkSTAR framework denoted by EKF-Kernel1. For a timestamp t , EKF-Kernel computes the priori state and covariance estimates $\hat{x}_{t|t-1}, P_{t|t-1}$ as well as the resulting residuals r_t using Equations (1), (3) and (2) respectively. Using Equation (4), the kernel estimates the innovation or the residual covariance matrix S_t . Next, the KRC-Kernel is invoked to validate the consistency of the Kalman gain matrix K_t with respect to the Jacobian H_t , the residual covariance S_t , as well as the posteriori covariance $P_{t|t}$. Subsequently, the posteriori state and covariance estimates are updated according to Equations (6) and (7). The kernel returns the current residual r_t , the residual covariance S_t and the Kalman reconstruction status κ_t .

Temporal Consistency (TC) Kernel: While the EKF kernel can enforce state space dynamics for each timestamp t , it cannot independently ensure the integrity of state space estimates across multiple time stamps. In order to do so, we need a mechanism to assert the integrity between distinct

timestamps. Therefore, we develop a temporal consistency (TC) kernel that is geared towards ensuring the integrity across distinct timestamps. Using the temporal decomposition scheme highlighted in Section 5.1 we focus on a single TC interval denoted by w to aid our discussion. We denote the inputs to the TC kernel in terms of three sets: \mathcal{X}_{w-1}^{TC} , \mathcal{R}_{w-1}^{TC} and \mathcal{K}_{w-1}^{TC} which represent state, residual and KRC status estimates from the previous TC interval $w-1$.

$$\mathcal{X}_{w-1}^{TC} = \underbrace{\{(x_{w-1|w-1} || N_{w-1}^x), (P_{w-1|w-1} || N_{w-1}^P)\}}_{\text{nonce appended state estimates}} \quad (14)$$

$$\mathcal{R}_{w-1}^{TC} = \underbrace{(r_{w-1} || N_{w-1}^r), (S_{w-1} || N_{w-1}^S)}_{\text{nonce appended residual and covariance}} \quad (15)$$

$$\mathcal{K}_{w-1}^{TC} = \underbrace{(\kappa_{w-1} || N_{w-1}^\kappa)}_{\text{nonce appended KRC status}} \quad (16)$$

Each set in turn consists of the raw values that are appended with a unique randomly chosen nonce value to provide a robust degree of entropy to the resulting hash strings. As a result, \mathcal{X}_{w-1}^{TC} consists of $(x_{w-1|w-1} || N_{w-1}^x), (P_{w-1|w-1} || N_{w-1}^P)$ where $x_{w-1|w-1}$, $P_{w-1|w-1}$, N_{w-1}^x and N_{w-1}^P denote the posteriori state and covariance estimate and their corresponding nonce values from the previous TC interval. Similarly, \mathcal{R}_{w-1}^{TC} comprises the residual and covariance pairs $(r_{w-1} || N_{w-1}^r)$ and $(S_{w-1} || N_{w-1}^S)$, where r_{w-1} and S_{w-1} represent the innovation and its associated covariance from the previous window, and N_{w-1}^r and N_{w-1}^S are the corresponding nonce values ensuring stochastic uniqueness of their hash representations. Finally, \mathcal{K}_{w-1}^{TC} encapsulates $(\kappa_{w-1} || N_{w-1}^\kappa)$, where κ_{w-1} denotes the binary KRC indicator and N_{w-1}^κ is its

appended nonce value used to prevent deterministic linkage across temporal proofs.

$$\mathcal{Z}_t^{TC} = \underbrace{\{(y_t || N_t^y), (G_t || N_t^G), (H_t || N_t^H), (K_t || N_t^K)\}}_{\text{nonce appended sensor data, Jacobian and Kalman Gain}} \quad (17)$$

$$\mathcal{Z}_w^{TC} = \underbrace{\{\mathcal{Z}_{t_w}^{TC}, \mathcal{Z}_{t_w+1}^{TC}, \dots, \mathcal{Z}_{t_w+D}^{TC}\}}_{\text{EKF inputs for TC interval } w} \quad (18)$$

Additionally, the TC kernel also utilizes the set \mathcal{Z}_w^{TC} which encapsulates the offline computed inputs and sensor data denoted by \mathcal{Z}_t^{TC} meant for the EKF Kernel invocations at each timestep of the TC interval. The set \mathcal{Z}_t^{TC} contains the nonce-appended sensor measurements and model parameters $(y_t || N_t^y)$, $(G_t || N_t^G)$, $(H_t || N_t^H)$, and $(K_t || N_t^K)$ corresponding to the sensor data, the Jacobians, and Kalman gain, respectively. Each element in \mathcal{Z}_t^{TC} is locally randomized through its associated nonce to ensure that the resulting hashed representations remain unlinkable across successive EKF invocations. Collectively, the windowed set \mathcal{Z}_w^{TC} aggregates these per-timestep inputs over the duration of the TC interval w , thereby serving as the complete batch of EKF inputs required for evaluating the zkSTAR TC kernel and generating the proof of temporal consistency for that interval. Consequently, Equation (19) is used to represent the TC kernel as a mapping denoted by \mathcal{M}^{TC} .

$$\begin{aligned} \mathcal{M}^{TC} : \mathcal{I}_{t_w}^{TC} = & \underbrace{\{[\mathcal{X}, \mathcal{R}, \mathcal{K}]_{w-1}, [\mathcal{Z}, \mathcal{N}]_w\}}_{\text{input for TC interval } w} \mapsto \\ & \mathcal{O}_{t_w}^{TC} = \underbrace{\{[\mathcal{X}, \mathcal{R}, \mathcal{K}]_w\}}_{\text{output of TC interval } w}. \end{aligned} \quad (19)$$

Algorithmically, the kernel is represented using the

Algorithm 3 zkSTAR Temporal Consistency (TC) Kernel

```

1: function TC-KERNEL( $\mathcal{X}_{w-1}^{TC}, \mathcal{R}_{w-1}^{TC}, \mathcal{Z}_w^{TC}, \mathcal{N}_w^{TC}$ )
2: #Strip nonce vectors from inputs
3:  $\{x_{t_w-1|t-1}, P_{t_w-1|t_w-1}\} \leftarrow \text{STRIPNONCE}(\mathcal{X}_{w-1}^{TC})$ 
4:  $\{r_w, S_w, \kappa_w\} \leftarrow \text{STRIPNONCE}(\mathcal{R}_{w-1}^{TC})$ 
5:  $\{y_t, G_t, H_t, K_t\}_{t_w+D}^{t_w+D} \leftarrow \text{STRIPNONCE}(\mathcal{Z}_w^{TC})$ 
6: for  $t \in \{t_w, t_w+1, t_w+2 \dots t_w+D\}$  do
7:  $\mathcal{X}_{t-1} \leftarrow \{x_{t-1|t-1}, P_{t-1|t-1}\}$ 
8:  $\mathcal{J}_t \leftarrow \{G_t, H_t, K_t\}$ 
9:  $\mathcal{O}_t^{EKF} \leftarrow \text{EKF-KERNEL}(\mathcal{X}_{t-1}, y_t, \mathcal{J}_t)$ 
10: accumulate residual sum  $r_w \leftarrow r_w + r_t$ 
11: accumulate residual covariance sum  $S_w \leftarrow S_w + S_t$ 
12: accumulate KRC status  $\kappa_w \leftarrow \kappa_w \circ \kappa_t$ 
13: end for
14: #Append nonce strings from  $\mathcal{N}_w^{TC}$ 
15:  $\mathcal{X}_w^{TC} \leftarrow \{(x_{t_w+D|t+D} || N_w^x), (P_{t_w+D|t_w+D} || N_w^P)\}$ 
16:  $\mathcal{R}_w^{TC} \leftarrow \{(r_w || N_w^r), (S_w || N_w^S)\}$ 
17:  $\mathcal{K}_w^{TC} \leftarrow (\kappa_w || N_w^K)$ 
18: return  $\mathcal{X}_w^{TC}, \mathcal{R}_w^{TC}, \mathcal{K}_w^{TC}$ 
19: end function

```

TC-Kernel function presented in Algorithm 3. The kernel

consumes the outputs of the previous TC interval $w-1$ and iterates through the timestamps $\{t_w \dots t_w+D\}$ belonging to the current TC interval w . For each timestamp, the kernel strips the nonce vectors to obtain the underlying values which are fed to EKF-Kernel. The residual, covariance and KRC status outputs of the EKF kernel are accumulated across all the timestamps of the current TC interval w through summation and multiplication operations respectively. At each iteration, the kernel returns the overall outputs pertaining to the state, residual and reconstruction status check for the corresponding TC interval.

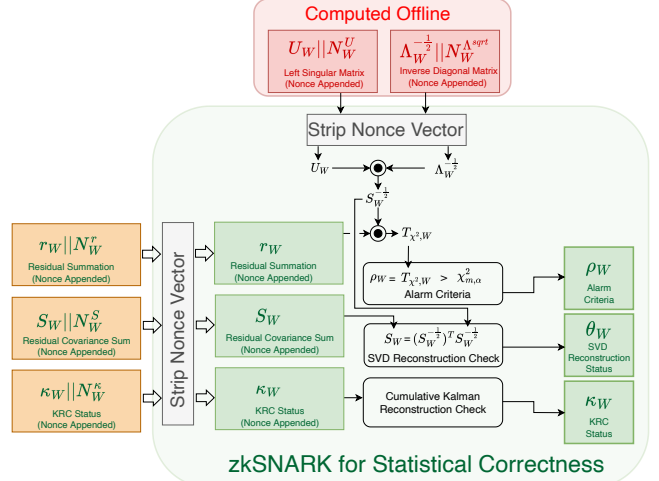


Figure 2: Statistical consistency estimation in zkSTAR

5.3. zkSNARK based Statistical Kernels

Applying the χ^2 test on the accumulated residuals and covariance requires us to carry out SVD decomposition to evaluate the test statistic and the alarm criteria in complete zero-knowledge. Therefore, we design a sequence of statistical zkSNARK kernels to help achieve efficiency in zkSTAR. **SVD Reconstruction Kernel:** We develop a kernel to validate the SVD decomposition of the accumulated covariance matrix in zero-knowledge. The SVD step is essential to compute the normalized PC scores so as to determine the value of the test statistic in conjunction with the accumulated residual values for each detection window. The SVD validation kernel SVD-Kernel is presented in Algorithm 4. Specifically the SVD kernel consumes the offline computed

Algorithm 4 zkSTAR Kernel for SVD Reconstruction

```

1: function SVD-KERNEL( $U, \Sigma^{-\frac{1}{2}}, S, \epsilon$ )
2:  $\eta \leftarrow 0$ 
3: if  $\|(U\Sigma^{-\frac{1}{2}})^T(U\Sigma^{-\frac{1}{2}}) - S^T S\|_2^2 < \epsilon$  then  $\eta \leftarrow 1$ 
4: end if
5: return  $\eta$ 
6: end function

```

value of the left singular matrix U as well as the square root of the singular values $\Sigma^{-\frac{1}{2}}$, an error tolerance threshold ϵ in

addition to the accumulated covariance matrix S itself. The kernel returns the validation status η depending on whether the SVD reconstruction represented by $U(\Sigma^{-\frac{1}{2}})^T(U\Sigma^{-\frac{1}{2}})$ falls within an ϵ ball of the predicted covariance matrix accumulated across the detection window.

Hypothesis Test Kernel: We conduct the χ^2 hypothesis test using the SC-Kernel which considers the accumulated residual and covariance values at the end of every detection window. Additionally, we compute the SVD of the accumulated covariance matrix in an offline manner and validate its consistency using the SVD reconstruction kernel denoted by SVD-Kernel. We represent the inputs to the SVD kernel in terms of \mathcal{Z}_W^{SVD} as stated in Equation (20) which consists of the singular vectors and the square roots of the singular values.

$$\mathcal{Z}_W^{SVD} = \underbrace{\{(U_W || N_W^U), (\Sigma_W^{-\frac{1}{2}} || N_W^\Sigma)\}}_{\text{nonce appended SVD values}} \quad (20)$$

The hypothesis testing kernel pertaining to detection window W can therefore be denoted as a mapping \mathcal{M}_W^{SC} as stated in Equation (21) which maps input set \mathcal{I}_w^{SC} to output $\mathcal{O}_{t_w}^{SC}$.

$$\mathcal{M}^{SC} : \underbrace{\mathcal{I}_W^{SC} = \{\mathcal{R}_W, \mathcal{Z}_W^{SVD}\}}_{\text{input for HT}} \mapsto \underbrace{\mathcal{O}_{t_w}^{SC} = \{\rho_W, \eta_W, \kappa_W\}}_{\text{output of HT}} \quad (21)$$

In Equation (21), \mathcal{R}_W represents outputs of TC-Kernel obtained upon the culmination of the current detection window while \mathcal{Z}_W^{SVD} represents the offline computed SVD of the accumulated residual covariance matrix.

Algorithm 5 zkSTAR Kernel for the χ^2 Hypothesis Test

```

1: function SC-KERNEL( $\mathcal{R}_W, \mathcal{Z}_W^{SVD}$ )
2: #Strip nonce vectors from inputs
3:  $\{r_W, S_W, \kappa_W\} \leftarrow \text{STRIPNONCE}(\mathcal{R}_W)$ 
4:  $\{U_W, \Sigma_W^{-\frac{1}{2}}\} \leftarrow \text{STRIPNONCE}(\mathcal{Z}_W^{SVD})$ 
5: #Set UCL and default alarm for  $W$ 
6:  $T_W^{UCL} \leftarrow \chi_{m,\alpha}^2, \rho_W \leftarrow 0$ 
7:  $\eta_W \leftarrow \text{SVD-KERNEL}(U_W, \Sigma_W^{-\frac{1}{2}}, S_W, \epsilon_{SVD})$ 
8: compute  $T_{\chi^2, W} \leftarrow \|U_W \Sigma_W^{-\frac{1}{2}} r_W\|_2^2$ 
9: if  $T_{\chi^2, W} > \chi_{m,\alpha}^2$  then  $\rho_W \leftarrow 1$  then
10: end if
11: return  $\rho_W, \eta_W, \kappa_W$ 
12: end function
26:  $\Pi_t^{TC} \leftarrow \text{Prove}(pk^{TC}, \theta^{TC}, \mathcal{M}^{TC}, \mathcal{I}_j^{TC}, \mathcal{O}_j^{TC})$ 
27:
28: extract  $[\mathcal{X}, \mathcal{R}, \mathcal{K}]_j$  from  $\mathcal{O}_j^{TC}$ 
29: end for
30: extract  $S_W$  from  $\mathcal{R}_W$ 
31:  $U_W, \Sigma_W^{-\frac{1}{2}} \leftarrow \text{SVD}(S_W)$   $\triangleright$  computed offline
32: generate nonce values  $\mathcal{N}^{SVD}$ 
33: compute  $\mathcal{Z}_W^{SVD}$  using SVD values  $U_W, \Sigma_W^{-\frac{1}{2}}, \mathcal{N}^{SVD}$ 
34:  $[\rho, \eta, \kappa]_W \leftarrow \text{SC-KERNEL}(\mathcal{R}_W, \mathcal{Z}_W^{SVD})$ 
35:
36: #Generate SC proof for window  $\mathcal{W}_i$ 
37:  $\Pi_t^{SC} \leftarrow \text{Prove}(pk^{SC}, \theta^{SC}, \mathcal{M}^{SC}, \mathcal{I}_W^{SC}, \mathcal{O}_W^{SC})$ 
38:

```

In SC-Kernel represented in Algorithm 5, we consume \mathcal{R}_W and \mathcal{Z}_W^{SVD} and initiate the hypothesis testing procedure by stripping the nonce vectors from the inputs. We compute the test statistic $T_{\chi^2, W}$ by utilizing the offline computed SVD values. Additionally, the value of the upper control limit T_W^{UCL} is baked into the proving circuit for individual subsystems since it is assumed to remain invariant across time, while the alarm value ρ_W is set to 0 by default. We compare the test statistic with T^{UCL} to determine the value of ρ_W within the kernel. Lastly, the SVD kernel is invoked to ensure the consistency of the offline computed

SVD values with the accumulated sensor covariance matrix S_W with a threshold of ϵ_{SVD} to yield a consistency status denoted by η_W . The kernel outputs a tuple of values consisting of the alarm ρ_W , the SVD status check η_W as well as the cumulative KCR status check of κ_W .

Algorithm 6 zkSTAR Algorithmic Framework

```

1: #Set visibility for TC circuit
2: #input;output;param visibility
3: hash;hash;private←PROVINGMODE( $\mathcal{M}^{TC}$ )
4:
5: #Setup proving circuit for TC
6: Setup( $1^\lambda, \mathcal{M}^{TC}, \theta^{TC}$ )  $\mapsto (pk^{TC}, vk^{TC})$ 
7:
8: #Set visibility for SC circuit
9: #input;output;param visibility
10: hash;public;private←PROVINGMODE( $\mathcal{M}^{SC}$ )
11:
12: #Setup proving circuit for SC
13: Setup( $1^\lambda, \mathcal{M}^{SC}, \theta^{SC}$ )  $\mapsto (pk^{SC}, vk^{SC})$ 
14:
15: distribute  $vk^{TC}, vk^{SC}$  publicly
16:
17: for  $i = 1, 2 \dots \text{do}$   $\triangleright$  rolling detection windows  $\mathcal{W}_i$ 
18:   for  $j = 1, 2, \dots W \text{ do}$   $\triangleright$  TC interval  $w_{ij}$ 
19:     generate nonce values  $\mathcal{N}_j^{TC}$ 
20:     compute  $\mathcal{Z}_j^{TC}$  using Equation (18)
21:     compute  $[\mathcal{X}, \mathcal{R}, \mathcal{K}]_{j-1}$  using Equations (14)-(16).
22:      $\mathcal{I}_j^{TC} \leftarrow \{[\mathcal{X}, \mathcal{R}, \mathcal{K}]_{j-1}, [\mathcal{Z}^{TC}, \mathcal{N}^{TC}]_j\}$ 
23:      $\mathcal{O}_j^{TC} \leftarrow \text{TC-KERNEL}(\mathcal{I}_j^{TC})$ 
24:
25:     #Generate TC proof for interval  $j$ 
26:      $\Pi_t^{TC} \leftarrow \text{Prove}(pk^{TC}, \theta^{TC}, \mathcal{M}^{TC}, \mathcal{I}_j^{TC}, \mathcal{O}_j^{TC})$ 
27:
28:     extract  $[\mathcal{X}, \mathcal{R}, \mathcal{K}]_j$  from  $\mathcal{O}_j^{TC}$ 
29:   end for
30:   extract  $S_W$  from  $\mathcal{R}_W$ 
31:    $U_W, \Sigma_W^{-\frac{1}{2}} \leftarrow \text{SVD}(S_W)$   $\triangleright$  computed offline
32:   generate nonce values  $\mathcal{N}^{SVD}$ 
33:   compute  $\mathcal{Z}_W^{SVD}$  using SVD values  $U_W, \Sigma_W^{-\frac{1}{2}}, \mathcal{N}^{SVD}$ 
34:    $[\rho, \eta, \kappa]_W \leftarrow \text{SC-KERNEL}(\mathcal{R}_W, \mathcal{Z}_W^{SVD})$ 
35:
36:   #Generate SC proof for window  $\mathcal{W}_i$ 
37:    $\Pi_t^{SC} \leftarrow \text{Prove}(pk^{SC}, \theta^{SC}, \mathcal{M}^{SC}, \mathcal{I}_W^{SC}, \mathcal{O}_W^{SC})$ 
38:
39:   return  $\mathcal{P}_{\mathcal{W}_i} = \left[ \left( \Pi_{w_{i1}}^{TC} \dots \Pi_{w_{iW}}^{TC} \right), \Pi_{\mathcal{W}_i}^{SC} \right]$ 
40: end for

```

5.4. zkSTAR Algorithmic Framework

We describe the overall zkSTAR algorithmic framework in Algorithm 6 that encapsulates the TC and SC kernels. The framework primarily executes on a rolling horizon of detection windows characterized by \mathcal{W}_i with each window consisting of W TC intervals of D timestamps each.

As a result, zkSTAR produces W TC and 1 SC proof artifact for each detection window \mathcal{W}_i which is denoted by

the set $\mathcal{P}_{\mathcal{W}_i}$ described in Equation (22).

$$\mathcal{P}_{\mathcal{W}_i} = \left[\left(\Pi_{w_{i1}}^{TC} \dots \Pi_{w_{iW}}^{TC} \right), \Pi_{\mathcal{W}_i}^{SC} \right] \quad (22)$$

Prior to execution, zkSTAR performs a setup phase to configure the proving environment for its two zkSNARK circuits: the Temporal Consistency (TC) and Statistical Consistency (SC) circuits. As shown in Algorithm 6, each circuit is first assigned a visibility mode through the PROVINGMODE routine. For the TC circuit, we adopt a *hash, hash, private* configuration that ensures that the proof artifact contains only the hashes of the input and output sets $\text{hash}(\mathcal{I}_w^{TC})$ and $\text{hash}(\mathcal{O}_w^{TC})$ while keeping model parameters private. Additionally the *hash, hash, private* visibility mode ensures that inputs and outputs remain hidden while preserving verifiable linkage across time steps. The setup procedure $\text{Setup}(1^\lambda, \mathcal{M}^{TC}, \theta^{TC})$ generates the proving and verification keys (pk^{TC}, vk^{TC}) . Meanwhile the SC circuit follows a slightly different configuration using *hash, public, private* implying that SC proof artifacts contain hashed input denoted by $\text{hash}(\mathcal{I}_w^{SC})$ and a public output \mathcal{O}_w^{SC} with private parameter visibility. As a result, we obtain (pk^{SC}, vk^{SC}) as the proving and verification keys for the SC circuit respectively. Both verification keys are then published for regulator verification. Following initialization, zkSTAR executes the runtime workflow in Algorithm 6, iterating over detection windows and TC intervals to generate nonce-protected inputs, invoke the TC-Kernel for temporal consistency, and apply the HT-Kernel for statistical validation, thereby producing verifiable, zero-knowledge proofs of system consistency.

For each detection window \mathcal{W}_i , the algorithm iterates through the TC intervals w_{ij} of length W . Within each TC interval, a fresh set of nonce values \mathcal{N}_j^{TC} is generated to enable efficient hiding for hash outputs. Using these nonces, the algorithm constructs the nonce-appended input set \mathcal{Z}_j^{TC} according to Equation (18), which encapsulates sensor data, model Jacobians, and Kalman gain parameters. The posterior state, residual, and kernel reconstruction variables from the previous interval, $[\mathcal{X}, \mathcal{R}, \mathcal{K}]_{j-1}$, are then obtained from (14)–(16). Together, these form the TC-kernel input $\mathcal{I}_j^{TC} = [\mathcal{X}, \mathcal{R}, \mathcal{K}]_{j-1}, [\mathcal{Z}^{TC}, \mathcal{N}^{TC}]_j$, which is passed to the TC-KERNEL for zkSNARK-based verification of temporal consistency. The kernel outputs the updated tuple $\mathcal{O}_j^{TC} = [\mathcal{X}, \mathcal{R}, \mathcal{K}]_j$, whose elements are extracted and propagated to the next interval.

After all W TC intervals within \mathcal{W}_i are processed, the accumulated residual set \mathcal{R}_W is used to derive the composite covariance S_W . An offline singular-value decomposition is then performed to obtain U_W and $\Sigma_W^{-\frac{1}{2}}$, which serve as normalized orthogonal bases for statistical calibration. A new nonce sequence \mathcal{N}^{SVD} is generated, and the nonce-augmented SVD feature set \mathcal{Z}_W^{SVD} is constructed accordingly. Finally, the SC-KERNEL consumes \mathcal{R}_W and \mathcal{Z}_W^{SVD} to compute the high-level decision metrics $[\rho, \eta, \kappa]_W$, representing the detection confidence, threshold statistics, and overall temporal-consistency verdict for the window \mathcal{W}_i . This output constitutes the verifiable zkSNARK-backed

anomaly indicator used by zkSTAR for secure, decentralized model validation.

5.5. Assumptions and Limitations

The zkSTAR framework relies on several assumptions pertaining to the properties of the zero-knowledge proving system. First, since zkSTAR uses the Halo2 proof generation paradigm as a consequence of using the `ezk1` framework [37], it implicitly depends on elliptic-curve cryptographic primitives and on the integrity of the Common Reference String (CRS). As a result, we assume that the CRS is generated through a publicly verifiable ceremony per-utility. Second, we assume that the EKF model is well-formed and is strongly sensitive to the Jacobian matrices [38] implying that slight deviations in SVD or Kalman gain computations would lead to inconsistent state and residual estimates violating either TC or SC conditions. Third, we assume that verifier is honest-but-curious and that public values of the proof artifacts do not violate privacy of utility state space which is a common requirement of existing regulators [39]. Finally, we assume that communication channels are assumed to preserve integrity but not confidentiality which can be alleviated by using transport-level encryption like TLS for privacy during proof transmission. Under these assumptions, zkSTAR achieves end-to-end regulatory verification with cryptographic soundness and provable privacy, while maintaining computational feasibility for real-world industrial deployments.

6. Experimental Results

For experimental studies, we utilize the HAI [40] and ORNL-PS [41], [42] datasets. To build an asset level anomaly detector, we generate pretrained non-linear models using the EKF approach to accurately reflect the state-space of the critical asset subsystems as described in Section 3. The training methodology for EKF models is briefly discussed in Appendix A.2. We encode the temporal and statistical components of these models in corresponding zkSNARKs as described in previous sections. As a result, the zkSTAR framework encodes temporal and statistical consistency with respect to detection outcomes.

We carry out detection based on a pre-determined value of upper control limit (UCL) that is representative of the levels of significance used for the χ^2 hypothesis test. These UCL values are generally dependent on the subsystem data and might also rely on engineering domain expertise as well. We use a value of $5e-3$ and $2e-2$ for HAI and ORNL-PS datasets that were obtained after rigorous empirical studies. All of our results include comparison with the non-ZKP version as our benchmark to judge the detection quality.

System Implementation Details: All experiments were carried out on a virtual machine (VM) running Ubuntu 24.04 with 100GB of RAM and 16 vCPUs using Python 3.11 with the detection model inference using PyTorch 2.7.1. We utilize the `ezk1` library [37] for generating all the zkSNARKs associated with the zkSTAR framework. We implement zkSTAR using both native and containerized execution modes. The native mode targets high-performance

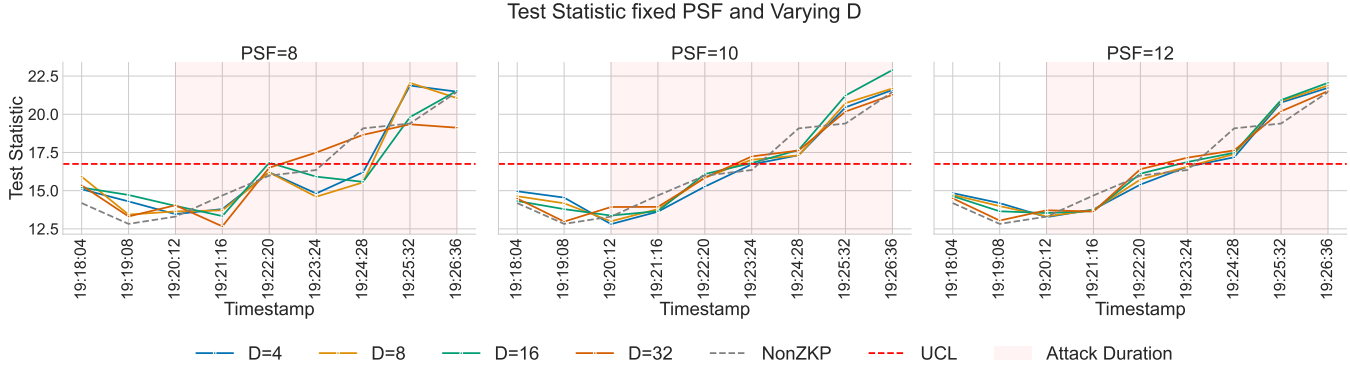


Figure 3: HAI Dataset: Detection Quality with varying D and fixed PSF

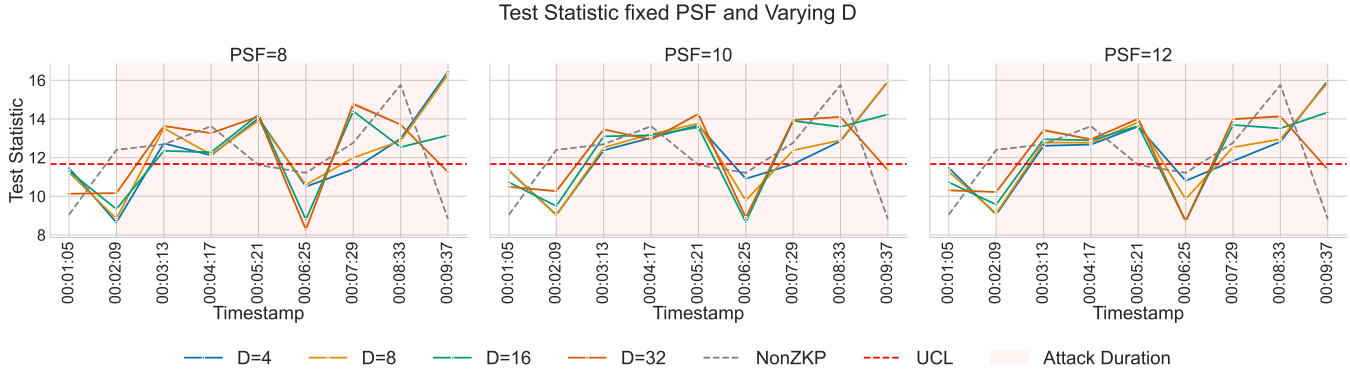


Figure 4: ORNL-PS Dataset: Detection Quality with varying D and fixed PSF

computing (HPC) clusters for evaluating detection accuracy and computational correctness across varying residual aggregation windows (D) and precision scale factors (PSF). The containerized mode assesses real-world performance, including CPU and memory usage during witness generation and TC and SC proof generation and verification. Separate containers emulate the utility (prover) and regulator (verifier), communicating via REST APIs and managed through the `zkstarctl` command-line interface.

6.1. Detection Quality of zkSNARK outcomes

To evaluate detection quality, we conduct two experiments examining the effects of varying the PSF with fixed D and vice versa. For brevity, PSF variation results are shown in Appendix C.2. Each experiment spans a 10-minute detection window, with attacks initiated mid-run. For HAI, the attack window includes the actual 164s event and a 3-minute buffer to account for the non-linear model’s delayed anomaly convergence, whereas in ORNL-PS, the attack persists until the end of the run. We test PSF values of 8, 10, and 12, and D values of 4, 8, 16, and 32.

Figures 3 and 4 demonstrate the detection quality with varying D and while fixing the PSF values to 8, 10 and 12 respectively. From both figures we can observe that the detection quality with respect to the UCL remains robust across varying values of D and PSF. Generally, we can

observe from both figures that the curves for different D values become more clustered around the non-zkSNARK version with increasing PSF values. This trend remains consistent across both datasets as well. In each case we can observe that the detection consistently occurs within the designated attack duration window providing similar quality as the non-ZKSNAK version.

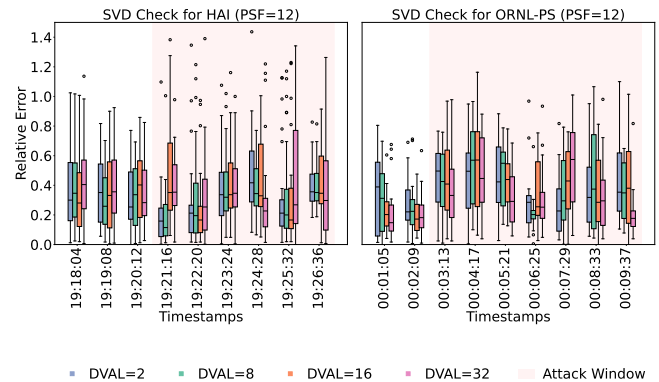


Figure 5: Computational error check for SVD of Kalman gain and aggregated covariance matrices

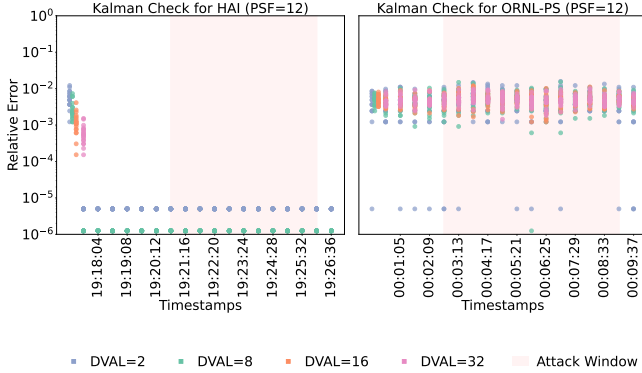


Figure 6: Computational error check for SVD of Kalman gain and aggregated covariance matrices

| Dataset | PK | VK | PF |
|---------|----------------------|---------------|---------------|
| HAI | 16011.879 (2271.245) | 3.878 (1.014) | 0.039 (0.004) |
| ORNL-PS | 16516.104 (2735.173) | 4.103 (1.221) | 0.040 (0.006) |

TABLE 1: TC Circuit: Proof (PF), Proving Key (PK), and Verification Key (VK) sizes for TC (mean(std) in MB)

6.2. Computational Correctness of zkSTAR output

The SVD and Kalman gain decompositions in the zkSTAR framework are computed offline. As a result, the zkSTAR framework outputs the reconstruction error, the associated threshold and a compute check flag for the SVD and Kalman gain matrices. We define the computational correctness as the absolute error emanating from the in-circuit reconstruction of the SVD and Kalman gain matrices computed with respect to the circuit encoded thresholds. Therefore, these experiments demonstrate the variation in relative absolute errors of all matrix elements with respect to the given threshold. In our experiments the threshold values for Kalman and SVD checks were set to 0.1.

Figure 5 shows box plots of relative error for varying D values on the HAI and ORNL-PS datasets (PSF = 12) based on the SVD of predicted covariance matrices. For both datasets, relative errors remain below 1 in most cases, indicating reconstruction errors under 0.1. Slight error spikes above 1 occur during attack windows due to increased residual volatility, yet even in the worst case, relative errors stay below 1.4 (HAI) and 1.2 (ORNL-PS). Figure 6 shows scatter plots of relative errors across varying D values. Unlike the SVD check, the Kalman gain check, which is performed every D steps, exhibits an initial staggered trend. For the HAI dataset, errors remain consistently low around $1e - 5$, while for the ORNL-PS dataset they are slightly higher yet stable, around $1e - 2$.

6.3. System Performance of Utility Prover

We begin by analyzing the system performance of zkSTAR proving system. Specifically, we examine the witness, proof, key and circuit sizes in addition to analyzing the utility's system performance of witness proof generation.

| Dataset | PK | VK | witness | Circuit Size | PF |
|---------|-------|-------|---------|--------------|-------|
| HAI | 12931 | 3.002 | 0.023 | 0.009 | 0.037 |
| ORNL-PS | 12931 | 3.002 | 0.016 | 0.008 | 0.035 |

TABLE 2: SC Circuit Proof (PF), Proving Key (PK), and Verification Key (VK) sizes for SC in MB)

| D Value | HAI | | ORNL-PS | |
|---------|--------------|---------|--------------|---------|
| | Witness | Circuit | Witness | Circuit |
| 1 | 0.043(0.001) | 0.25 | 0.036(0.002) | 0.24 |
| 4 | 0.073(0.001) | 0.78 | 0.064(0.001) | 0.78 |
| 8 | 0.114(0.001) | 1.50 | 0.101(0.001) | 1.49 |
| 16 | 0.197(0.001) | 2.94 | 0.176(0.002) | 2.93 |
| 32 | 0.362(0.002) | 5.82 | 0.325(0.004) | 5.80 |

TABLE 3: Temporal Consistency Witness Size with Varying D (mean(std) in MB)

Analysis of Proof and Key Sizes: Tables 1 and 2 presents the sizes of the proof, proving and verification keys for the temporal consistency and statistical consistency proofs. Table 2 also presents the witness size pertaining to the statistical consistency proofs. Additionally, we present the witness and the compiled circuit size for temporal consistency proofs for PSF value 8 separately in Table 3.

In Table 1, we can observe that for the case of temporal consistency, the proof size as well as proving and verification key sizes are similar for both datasets. On the other hand, in Table 2, the circuit, proving and verification key size for the statistical consistency proofs were constant as expected and minor deviations are observed for the proof and witness sizes across both datasets. However, we observe an interesting trend with respect to witness and circuit sizes as represented in Table 3. Mean witness sizes increase gradually from around 43kB to 360kB for HAI and 36kB to 325kB for ORNL-PS. On the other hand, the circuit sizes increase from a smaller value of 0.25MB at D value of 1 to 5.8MB for HAI while exhibiting a near identical trend for ORNL-PS dataset as well. This trend is natural and expected since increase in D value corresponds to larger TC interval sizes making the TC circuit grow exponentially.

Computational Analysis of Proving System: We analyze the computational performance for temporal and statistical consistency proof generation for both datasets for varying D values. Circuit generation and setup costs are presented separately in Appendix C.4. Our results are presented in Tables 4 and 5 for HAI and ORNL-PS datasets respectively. The data for these experiments are obtained from multiple runs of varying PSF values and represent the mean and standard deviation for one proof invocation of the circuit. We also provide a speed up value that represents the average case speedup that can be expected when sequentially generating proofs for the entire horizon. We provide the speedup formula and its associated explanation using Equation (48) in Appendix C.1 respectively.

The temporal consistency proof generation times are represented by the mean and standard deviation values for D values of 1,4,8 and 16. The proving times are in general stable with minor variations observed with varying D values. We observe that in case of HAI, the mean proof generation

| PSF Value | Hypothesis Test | D=1 | | D=4 | | D=8 | | D=16 | |
|-----------|-----------------|-------------|---------|-------------|---------|-------------|---------|-------------|---------|
| | | Time (s) | Speedup |
| 8 | 56.06(22.60) | 70.05(3.03) | 1.00 | 80.81(4.19) | 3.5 | 70.61(2.87) | 7.93 | 78.25(3.75) | 14.32 |
| 10 | 54.26(19.17) | 69.26(3.22) | 1.00 | 71.32(3.22) | 3.89 | 75.97(8.88) | 7.3 | 77.11(5.01) | 14.37 |
| 12 | 53.49(6.60) | 69.89(3.77) | 1.00 | 66.50(2.34) | 4.20 | 74.59(3.19) | 7.5 | 77.79(3.90) | 14.37 |

TABLE 4: HAI Dataset: Speedup and Proof Generation Times (mean (std) in seconds)

| PSF Value | Hypothesis Test | D=1 | | D=4 | | D=8 | | D=16 | |
|-----------|-----------------|--------------|---------|--------------|---------|--------------|---------|--------------|---------|
| | | Time (s) | Speedup |
| 8 | 49.01 (9.68) | 81.74 (2.85) | 1.00 | 57.75 (1.35) | 5.66 | 67.69 (1.74) | 9.66 | 72.64 (1.77) | 18.0 |
| 10 | 50.79 (1.32) | 69.82 (2.29) | 1.00 | 65.06 (1.17) | 4.29 | 68.66 (1.75) | 8.13 | 73.28 (1.83) | 15.24 |
| 12 | 52.40 (37.36) | 69.27 (3.99) | 1.00 | 64.45 (1.26) | 4.29 | 67.21 (1.22) | 8.24 | 73.32 (2.17) | 15.11 |

TABLE 5: ORNL-PS Dataset: Speedup and Proof Generation Times (mean (std) in seconds)

time increases slightly going from D values of 1 to 4 before decreasing slightly from 4 to 8 and finally increasing from 8 to 16. On the other hand the trend is inverted for ORNL-PS, decreasing slightly from 1 to 4, increasing from 4 to 8 and then decreasing again from 8 to 16. Interestingly, there is more volatility for PSF value of 8 in case of either dataset as compared to 10 and 12. The non-monotonous trends depicted in Tables 4 and 5 can be due to the non-linear proving costs afforded by `ezkl` backend which could be explained on the basis of row domain padding used by Halo2 proving systems. Further, analyzing speedups, we note a healthy increase between each set of D values regardless of the PSF value or the dataset used. Since the circuit size is known to influence the proving times, the trends in Tables 4 and 5 are exactly aligned with those depicted in Table 3. The speedup value insights point to the fact that having a higher TC interval size (or D value) is almost always more computationally efficient than invoking proof generation on a finer granularity corresponding to a lower TC interval size.

Lastly, the hypothesis test columns in Tables 4 and 5 reflect a relatively stable values of average proving time corresponding to statistical consistency proofs. These values are slightly higher for HAI compared to ORNL-PS which might be explained on the basis of the difference in dimensionality between both problems.

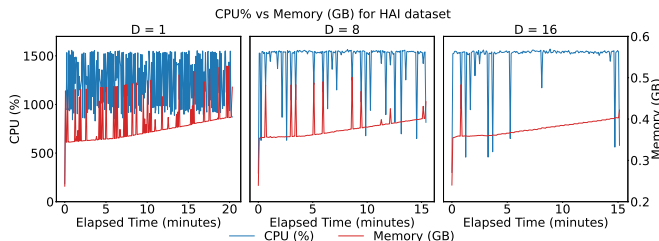


Figure 7: Witness Generation Performance with varying D for HAI dataset

System Performance of Witness and Proof Generation: Figures 7 and 8 present trends pertaining to the CPU utilization and memory consumption for only the HAI dataset. We provide the corresponding trends for ORNL-PS in Appendix C.3 due to space constraints. The results show a steady and predictable scaling trend, with CPU utilization peaking around 1600%, demonstrating effective parallelization, and

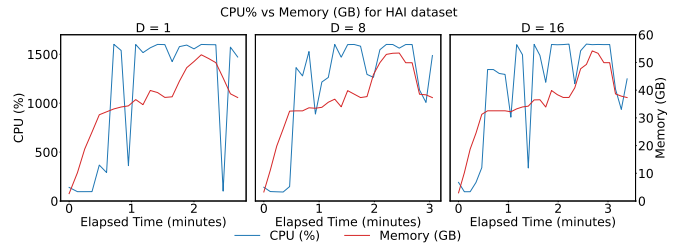


Figure 8: Prover Performance for Temporal Consistency with varying D for HAI dataset

memory usage reaching approximately 55 GB, well within available system capacity. From Figure 7, we can see greater volatility in CPU utilization and memory consumption for D value of 1 eventually stabilizing for D values of 8 and 16. The underlying reason for this trend is that lower values of D demand more frequent proving steps that results in higher volatility in CPU utilization and memory consumption. As D grows to 8 and 16, the proving time stabilizes on account of less frequent proving steps encountered during the simulation horizon. These results confirm that zkSTAR efficiently leverages multi-core resources with stability in memory consumption under increasing computational load.

Verification Latency: To gauge the regulatory overhead in terms of verification, we measure the verification times incurred by the regulator for verifying TC and SC proof artifacts. In almost all cases, zkSTAR SC and TC proofs are successfully verified in under 1.5s for both datasets with varying TC interval sizes. Detailed results pertaining to verification times for each case has been presented in Appendix C.5. These results assert the practicality of zkSTAR for near real-time regulatory audits with minimal overhead.

7. Conclusion

In this paper, we address the problem of regulatory compliance in data-driven cyberattack detection for utility stakeholders within large-scale Critical Infrastructure Networks (CINs). Privacy and efficiency constraints make full-fledged ICS data audits impractical, creating a key challenge for regulators seeking trustworthy verification of local detection outcomes. The absence of private, verifiable mechanisms can degrade network-wide situational awareness and

increase false positives, resulting in unnecessary downtimes.

To overcome these limitations, we present zkSTAR, a zkSNARK-based framework that enables publicly verifiable attack detection while preserving complete zero knowledge of local ICS state-space dynamics. zkSTAR provides formal guarantees of temporal and statistical consistency for utility-level detections, linking proof verification directly to the authenticity of attack alarms. We theoretically prove knowledge-soundness claims in zkSTAR while demonstrating its robustness to attack suppression in case of compromised utilities. For scalability, the framework decomposes proof generation into distinct zkSNARK-based kernels, ensuring computational efficiency and modularity.

We evaluate zkSTAR on a containerized testbed using real-world datasets from HAI and ORNL-PS, demonstrating robust performance across varying TC intervals and precision scales. System-level analysis further confirms the framework's stability in terms of CPU and memory utilization. Overall, our results show that zkSTAR enables secure, privacy-preserving, and publicly verifiable cyberattack detection suitable for diverse CIN deployment scenarios.

References

- [1] J. V. Cuffari, "Additional progress needed to improve information sharing under the cybersecurity act of 2015." <https://www.oig.dhs.gov/sites/default/files/assets/2022-08/OIG-22-59-Aug22.pdf>, 2022.
- [2] R. Langner, "Stuxnet: Dissecting a cyberwarfare weapon," *IEEE Security & Privacy*, vol. 9, no. 3, pp. 49–51, 2011.
- [3] B. Jeffries, S. Saravia, C. Carter, and Z. Ankuda, "Cyber risk to mission case study: Triton." <https://apps.dtic.mil/sti/html/trecms/AD1183008/>, 2022.
- [4] L. Salazar, S. R. Castro, J. Lozano, K. Koneru, E. Zambon, B. Huang, R. Baldick, M. Krotofil, A. Rojas, and A. A. Cardenas, "A tale of two industry destroyers: It was the season of darkness," in *2024 IEEE Symposium on Security and Privacy (SP)*, pp. 312–330, IEEE, 2024.
- [5] A. Nolan, *Cybersecurity and information sharing: Legal challenges and solutions*, vol. 5. Congressional Research Service, 2015.
- [6] D. Li, N. Gebraeel, and K. Paynabar, "Detection and differentiation of replay attack and equipment faults in scada systems," *IEEE Transactions on Automation Science and Engineering*, vol. 18, no. 4, pp. 1626–1639, 2020.
- [7] D. Li, P. Ramanan, N. Gebraeel, and K. Paynabar, "Deep learning based covert attack identification for industrial control systems," *arXiv preprint arXiv:2009.12360*, 2020.
- [8] M. Caselli, E. Zambon, J. Amann, R. Sommer, and F. Kargl, "Specification mining for intrusion detection in networked control systems," in *USENIX Security Symposium*, pp. 791–806, 2016.
- [9] N. Ye, Y. Zhang, and C. M. Borror, "Robustness of the markov-chain model for cyber-attack detection," *IEEE Transactions on Reliability*, vol. 53, no. 1, pp. 116–123, 2004.
- [10] D. I. Urbina, J. A. Giraldo, A. A. Cardenas, N. O. Tippenhauer, J. Valente, M. Faisal, J. Ruths, R. Candell, and H. Sandberg, "Limiting the impact of stealthy attacks on industrial control systems," in *Proceedings of the 2016 ACM SIGSAC Conference on Computer and Communications Security*, pp. 1092–1105, ACM, 2016.
- [11] D.-H. Kang, B.-K. Kim, and J.-C. Na, "Cyber threats and defence approaches in scada systems," in *16th International Conference on Advanced Communication Technology*, pp. 324–327, IEEE, 2014.
- [12] Z. Drias, A. Serhouchni, and O. Vogel, "Taxonomy of attacks on industrial control protocols," in *2015 International Conference on Protocol Engineering (ICPE) and International Conference on New Technologies of Distributed Systems (NTDS)*, pp. 1–6, IEEE, 2015.
- [13] T. Huang, B. Satchidanandan, P. Kumar, and L. Xie, "An online detection framework for cyber attacks on automatic generation control," *IEEE Transactions on Power Systems*, vol. 33, no. 6, pp. 6816–6827, 2018.
- [14] A. Hoehn and P. Zhang, "Detection of covert attacks and zero dynamics attacks in cyber-physical systems," in *American Control Conference (ACC), 2016*, pp. 302–307, IEEE, 2016.
- [15] M. S. Rahman, M. A. Mahmud, A. M. T. Oo, and H. R. Pota, "Multi-agent approach for enhancing security of protection schemes in cyber-physical energy systems," *IEEE Transactions on Industrial Informatics*, vol. 13, no. 2, pp. 436–447, 2017.
- [16] D. Li, K. Paynabar, and N. Gebraeel, "A degradation-based detection framework against covert cyberattacks on scada systems," *IEEE Transactions on Systems, Man, and Cybernetics: Systems*, vol. 53, no. 7, pp. 812–829, 2021.
- [17] P. Ramanan, D. Li, and N. Gebraeel, "Blockchain-based decentralized replay attack detection for large-scale power systems," *IEEE Transactions on Systems, Man, and Cybernetics: Systems*, vol. 52, no. 8, pp. 4727–4739, 2021.
- [18] D. Li, N. Gebraeel, K. Paynabar, and A. S. Meliopoulos, "An online approach to covert attack detection and identification in power systems," *IEEE Transactions on Power Systems*, vol. 38, no. 1, pp. 267–277, 2022.
- [19] A. Narayan, A. Feldman, A. Papadimitriou, and A. Haeberlen, "Verifiable differential privacy," in *Proceedings of the Tenth European Conference on Computer Systems*, pp. 1–14, 2015.
- [20] S. Goldwasser, S. Micali, and C. Rackoff, "The knowledge complexity of interactive proof-systems," in *Providing Sound Foundations for Cryptography: On the Work of Shafi Goldwasser and Silvio Micali*, pp. 203–225, 2019.
- [21] M. Blum, P. Feldman, and S. Micali, "Non-interactive zero-knowledge and its applications," in *Providing Sound Foundations for Cryptography: On the Work of Shafi Goldwasser and Silvio Micali*, pp. 329–349, 2019.
- [22] J. Kilian, "A note on efficient zero-knowledge proofs and arguments," in *Proceedings of the twenty-fourth annual ACM symposium on Theory of computing*, pp. 723–732, 1992.
- [23] S. Micali, "Computationally sound proofs," *SIAM Journal on Computing*, vol. 30, no. 4, pp. 1253–1298, 2000.
- [24] R. Gennaro, C. Gentry, B. Parno, and M. Raykova, "Quadratic span programs and succinct nizks without pcps," in *Advances in Cryptology–EUROCRYPT 2013: 32nd Annual International Conference on the Theory and Applications of Cryptographic Techniques, Athens, Greece, May 26–30, 2013. Proceedings 32*, pp. 626–645, Springer, 2013.
- [25] B. Parno, J. Howell, C. Gentry, and M. Raykova, "Pinocchio: Nearly practical verifiable computation," *Communications of the ACM*, vol. 59, no. 2, pp. 103–112.
- [26] E. Ben-Sasson, A. Chiesa, D. Genkin, E. Tromer, and M. Virza, "Snarks for c: Verifying program executions succinctly and in zero knowledge," in *Advances in Cryptology–CRYPTO 2013: 33rd Annual Cryptology Conference, Santa Barbara, CA, USA, August 18–22, 2013. Proceedings, Part II*, pp. 90–108, Springer, 2013.
- [27] C. Costello, C. Fournet, J. Howell, M. Kohlweiss, B. Kreuter, M. Naehrig, B. Parno, and S. Zahur, "Geppetto: Versatile verifiable computation," in *2015 IEEE Symposium on Security and Privacy*, pp. 253–270, IEEE, 2015.
- [28] E. Ben-Sasson, A. Chiesa, E. Tromer, and M. Virza, "Succinct {Non-Interactive} zero knowledge for a von neumann architecture," in *23rd USENIX Security Symposium (USENIX Security 14)*, pp. 781–796, 2014.
- [29] C. Huang, J. Wang, H. Chen, S. Si, Z. Huang, and J. Xiao, "zkmlaas: a verifiable scheme for machine learning as a service," in *GLOBECOM 2022–2022 IEEE Global Communications Conference*, pp. 5475–5480, IEEE, 2022.

- [30] H. Wang and T. Hoang, “ezdps: An efficient and zero-knowledge machine learning inference pipeline,” *arXiv preprint arXiv:2212.05428*, 2022.
- [31] T. Nguyen and M. T. Thai, “Preserving privacy and security in federated learning,” *arXiv preprint arXiv:2202.03402*, 2022.
- [32] W. Yang, Y. Yin, G. Zhu, H. Gu, L. Fan, X. Cao, and Q. Yang, “Fedzkp: Federated model ownership verification with zero-knowledge proof,” *arXiv preprint arXiv:2305.04507*, 2023.
- [33] D. Froelicher, J. R. Troncoso-Pastoriza, J. S. Sousa, and J.-P. Hubaux, “Drynx: Decentralized, secure, verifiable system for statistical queries and machine learning on distributed datasets,” *IEEE Transactions on Information Forensics and Security*, vol. 15, pp. 3035–3050, 2020.
- [34] H. Coskun, F. Achilles, R. DiPietro, N. Navab, and F. Tombari, “Long short-term memory kalman filters: Recurrent neural estimators for pose regularization,” in *Proceedings of the IEEE International Conference on Computer Vision*, pp. 5524–5532, 2017.
- [35] W.-Y. Hwang, “Chi-square quantile-based multivariate variance monitoring for individual observations,” *Communications in Statistics-Simulation and Computation*, vol. 46, no. 7, pp. 5392–5409, 2017.
- [36] A. J. Menezes, P. C. van Oorschot, and S. A. Vanstone, *Handbook of Applied Cryptography*. CRC Press, 1996.
- [37] T. South, A. Camuto, and contributors, “ezkl: Zero-knowledge machine learning inference framework.” <https://github.com/zkondutu/ezkl>, 2024. Accessed: 2025-02-12.
- [38] G. P. Huang, A. I. Mourikis, and S. I. Roumeliotis, “Analysis and improvement of the consistency of extended kalman filter based slam,” in *2008 IEEE International Conference on Robotics and Automation*, pp. 473–479, IEEE, 2008.
- [39] “Energy sector cybersecurity preparedness.” <https://www.energy.gov/ceser/activities/cybersecurity-critical-energy-infrastructure/energy-sector-cybersecurity>.
- [40] H.-K. Shin, W. Lee, S. Choi, J.-H. Yun, and B.-G. Min, “Hai security datasets,” 2023.
- [41] S. Pan, T. Morris, and U. Adhikari, “Classification of disturbances and cyber-attacks in power systems using heterogeneous time-synchronized data,” *IEEE Transactions on Industrial Informatics*, vol. 11, no. 3, pp. 650–662, 2015.
- [42] S. Pan, T. Morris, and U. Adhikari, “Developing a hybrid intrusion detection system using data mining for power systems,” *IEEE Transactions on Smart Grid*, vol. 6, no. 6, pp. 3104–3113, 2015.
- [43] R. S. Smith, “A decoupled feedback structure for covertly appropriating networked control systems,” *IFAC Proceedings Volumes*, vol. 44, no. 1, pp. 90–95, 2011.
- [44] Y. Mo, R. Chabukswar, and B. Sinopoli, “Detecting integrity attacks on scada systems,” *IEEE Transactions on Control Systems Technology*, vol. 22, no. 4, pp. 1396–1407, 2014.
- [45] A. Teixeira, S. Amin, H. Sandberg, K. H. Johansson, and S. S. Sastry, “Cyber security analysis of state estimators in electric power systems,” in *49th IEEE Conference on Decision and Control (CDC), Atlanta, GA, DEC 15-17, 2010*, pp. 5991–5998, 2010.
- [46] Zcash Team, “Halo2: The halo2 zero-knowledge proving system.” <https://github.com/zcash/halo2>, 2023. Accessed: 2025-10-26.

Ethics Consideration

None

LLM Usage Considerations

LLMs were used solely for editorial purposes in the preparation of this manuscript (e.g., grammar refinement, stylistic polishing, and clarity improvements). All outputs were manually reviewed, verified, and edited by the authors to ensure technical accuracy and originality. No new ideas, data, or

analyses were introduced through the use of LLMs. The literature review, experimental design, results interpretation, and all conceptual contributions were conducted entirely by the authors.

Appendix A. Extended Kalman Filter Model and Training

A.1. EKF Modeling for ICS

Our state space modeling framework is based on the extended Kalman filter (EKF) modeling paradigm that is capable of handling non-linearities inherent in the state space process [34]. In order to represent the EKF model, we use a deep neural network driven strategy that consists of one feed-forward and three LSTM sub-modules. Specifically, we consider a sensor-driven non-linear system at time t , where $x_t \in R^m$ represents the latent space embedding, $u_t \in R^m$ represents the control action and $y_t \in R^d$ represents noisy sensor measurements from asset sensors.

$$x_{t+1} = g(x_{t-1}, u_{t-1}) + v_t, \quad (23)$$

$$y_t = h(x_t) + w_t, \quad (24)$$

In Equations (23), (24), g, h are the state transition and observation functions respectively. The process and measurement noises at time t are denoted by $v_t \in R^m$, and $w_t \in R^d$ respectively. The process and measurement noises follow multivariate normal distributions with zero mean implying that $v_t \sim N(0, Q_t)$, $w_t \sim N(0, R_t)$, where Q_t, R_t represent the covariance matrices respectively. Such a type of modeling framework has also been used extensively in prior art [43]–[45]. Figure 9 represents the dynamics of our LSTM based deep neural network that is specifically tailored to establish the extended Kalman filter model for ICS subsystems.

A.2. EKF training methodology

During the training phase, the efficacy of the model is assessed by comparing the estimated state $x_{t|t}$ against the ground-truth state x_t through a carefully constructed loss function. This function typically comprises a mean squared error (MSE) term to minimize the divergence between the estimated and true states. To ensure statistical robustness and numerical stability, regularization terms are incorporated to constrain the norms and conditioning of the covariance matrices Q_t and R_t , as well as the Kalman gain K_t . These constraints mitigate overfitting and foster consistent learning behavior across iterations.

The total loss is subsequently backpropagated through the model’s architecture via automatic differentiation techniques, enabling the optimization of all learnable parameters. This includes parameters embedded within the state transition function, the measurement function, and the covariance estimation modules. Through iterative training over sequential data, the KFLSTM model progressively refines its ability to encapsulate the system’s dynamic behavior and uncertainty propagation, aligning seamlessly with the theoretical underpinnings of non-linear Kalman filtering.

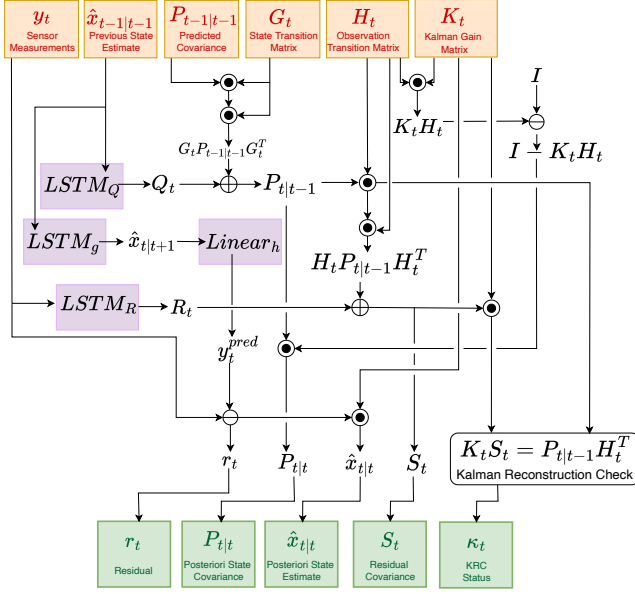


Figure 9: Non Linear Kalman Filter based Temporal State Estimation

Appendix B. Theorem and Lemma Proofs

B.1. Proof of Theorem 4.1

Proof. We know from Definition 3, for practical purposes \mathcal{H}_t^{out} and \mathcal{H}_t^{in} can be used to uniquely identify x_t^{out} and x_t^{in} . Therefore, it is sufficient to demonstrate the following

$$\mathcal{H}_{t+1}^{in} = \mathcal{H}_t^{out} \implies \Phi_{t+1} = 1 \quad (25)$$

$$\Phi_{t+1} = 1 \implies \mathcal{H}_{t+1}^{in} = \mathcal{H}_t^{out} \quad (26)$$

Case 1: Assume that for some $t, t+1$, there exists a $\tilde{x}_{t+1}^{in} \neq x_t^{out}$ such that $\Phi_{t+1} = 1$. Consequently, we can establish $\Delta_{t+1}^{in} = (\tilde{\mathcal{H}}_{t+1}^{in}, \tilde{x}_{t+1}^{in}, y_{t+1})$, where $\tilde{\mathcal{H}}_t^{in} = \text{hash}(x_{t+1}^{in})$. Using Definitions 5 and 6, we can obtain $\tilde{\Pi}_{t+1}, \tilde{\Phi}_{t+1}$ such that the following equation holds.

$$\tilde{\Pi}_{t+1} = \text{Prove}(pk, \theta, \mathcal{M}, \tilde{\Delta}_{t+1}^{in}, \tilde{\Delta}_{t+1}^{out}) \quad (27)$$

$$\tilde{\Phi}_{t+1} = \text{Verify}(vk, \tilde{\Pi}_{t+1}, \tilde{\Delta}_{t+1}^{in}, \tilde{\Delta}_{t+1}^{out}) \quad (28)$$

On the other hand, using \mathcal{H}_t^{out} , for verification purpose we can also construct $\Delta_{t+1}^{in} = (\mathcal{H}_t^{out}, \tilde{x}_{t+1}^{in}, y_t)$,

$$\Phi_{t+1} = \text{Verify}(vk, \tilde{\Pi}_{t+1}, \Delta_{t+1}^{in}, \tilde{\Delta}_t^{out}) \quad (29)$$

However, given $vk_t = vk_{t+1}$ and $pk_t = pk_{t+1}$, we know that $\Phi_{t+1} \neq \tilde{\Phi}_{t+1}$. As a result $\Phi_{t+1} \neq 1$ which presents a contradiction to our stated assumptions.

Case 2: Assume that for some $t+1$, $\Phi_{t+1} \neq 1$ such that $\mathcal{H}_{t+1}^{in} = \mathcal{H}_t^{out}$. Further let $\tilde{\Delta}_{t+1}^{in} = (\mathcal{H}_t^{out}, x_{t+1}^{in}, y_{t+1})$ and $\Delta_{t+1}^{in} = (\mathcal{H}_{t+1}^{in}, x_t^{out}, y_{t+1})$. Using Definition 2, we can assert that Δ_{t+1}^{in} and $\tilde{\Delta}_{t+1}^{in}$ are both valid inputs to \mathcal{M} parametrized by θ . Additionally, as a result of the

zk-SNARK verification property stated in Definition 6, we can also assert without loss of generality that there exist $\Pi_{t+1}, \Delta_{t+1}^{out}, \tilde{\Pi}_{t+1}, \tilde{\Delta}_{t+1}^{out}$ such that

$$\Phi_{t+1} = \text{Verify}(vk, \Pi_{t+1}, \Delta_{t+1}^{in}, \Delta_{t+1}^{out}) = 0 \quad (30)$$

$$\tilde{\Phi}_{t+1} = \text{Verify}(vk, \tilde{\Pi}_{t+1}, \tilde{\Delta}_{t+1}^{in}, \tilde{\Delta}_{t+1}^{out}) = 1 \quad (31)$$

Verification outcomes $\Phi_{t+1} = 0$ and $\tilde{\Phi}_{t+1} = 1$ will only be obtained in case of the following scenarios or a combination thereof.

Scenario 1 [$\Delta_{t+1}^{out} \neq \tilde{\Delta}_{t+1}^{out}$]: We know from Definition 2 that $\Delta_{t+1}^{out}, \tilde{\Delta}_{t+1}^{out}$ are deterministic outcomes from \mathcal{M} parametrized by θ . Therefore, it can be established that $\Delta_{t+1}^{out} \neq \tilde{\Delta}_{t+1}^{out}$ is a direct consequence of differing inputs to \mathcal{M} parametrized by θ . As a result, for this case, it holds that $\tilde{\Delta}_{t+1}^{in} \neq \Delta_{t+1}^{in}$ and as a consequence $\tilde{\Pi}_{t+1} \neq \Pi_{t+1}$ will also hold.

Scenario 2 [$\tilde{\Pi}_{t+1} \neq \Pi_{t+1}$]: We know that the following relationship must hold if $\tilde{\Phi}_{t+1} = 1$

$$\tilde{\Pi}_{t+1} = \text{Prove}(pk, \theta, \mathcal{M}, \tilde{\Delta}_{t+1}^{in}, \tilde{\Delta}_{t+1}^{out}) \quad (32)$$

Since, $\tilde{\Pi}_{t+1} \neq \Pi_{t+1}$, we can derive that either $\tilde{\Delta}_{t+1}^{in} \neq \Delta_{t+1}^{in}$ or $\Delta_{t+1}^{out} \neq \tilde{\Delta}_{t+1}^{out}$. We have already shown that $\Delta_{t+1}^{out} \neq \tilde{\Delta}_{t+1}^{out}$ directly results from $\tilde{\Delta}_{t+1}^{in} \neq \Delta_{t+1}^{in}$. As a result, it conclusively holds that $\tilde{\Delta}_{t+1}^{in} \neq \Delta_{t+1}^{in}$.

As a result, we establish that divergent verification outcomes $\Phi_{t+1} = 0$ and $\tilde{\Phi}_{t+1} = 1$ necessarily imply $\tilde{\Delta}_{t+1}^{in} \neq \Delta_{t+1}^{in}$. Therefore, $\mathcal{H}_{t+1}^{out} \neq \tilde{\mathcal{H}}_{t+1}^{in}$ and $x_{t+1}^{in} \neq \tilde{x}_{t+1}^{out}$ which is a contradiction to our stated assumption. \square

B.2. Proof of Lemma 1

Proof. We can see that under conditions of probabilistic similarity, the following holds

$$\tilde{T}_t > \chi_{p,\alpha}^2 \text{ and } \tilde{T}_t > \chi_{p,\alpha}^2 \quad (33)$$

From Section 3.2, we know that this leads to $\tilde{\rho}_t = \rho_t$ respectively thereby establishing the sufficiency argument.

On the other hand, under conditions of statistical consistency between $\tilde{\rho}_t, \rho_t$, there exists corresponding underlying measurement values \tilde{y}_t, y_t . Since we know that $\tilde{\rho}_t = \rho_t$, it is trivial to show that \tilde{y}_t, y_t lead to corresponding test statistic values \tilde{T}_t, T_t such that $\tilde{T}_t > \chi_{p,\alpha}^2$ and $T_t > \chi_{p,\alpha}^2$. This proves the necessity argument. \square

B.3. Proof of Theorem 4.2

Proof. We know from Theorem 4.1 that $\mathcal{H}_{t+1}^{in} = \mathcal{H}_t^{out}$, and $\Phi_{t+1} = 1$ is a necessary and sufficient condition for temporal consistency. Therefore, to prove this theorem, it is sufficient to show that for a temporally consistent system $\Phi_{t+1} = 1 \iff$ Statistical consistency.

(Case 1 $\Phi_{t+1} = 1 \implies$ Statistical consistency): Assume that $\rho_{t+1}^{real} \neq \rho_{t+1}^{rep}$ but $\Phi_{t+1} = 1$. Based on Lemma 1, we know that there are two probabilistically dissimilar sensor measurement realizations $y_{t+1}^{real}, y_{t+1}^{rep}$ corresponding to $\rho_{t+1}^{real}, \rho_{t+1}^{rep}$ respectively. This implies that there exists a

system of proof artifacts pertaining to ρ_{t+1}^{rep} that satisfy the following relations.

$$\tilde{\Delta}_{t+1}^{in} = (\tilde{\mathcal{H}}_{t+1}^{in}, \tilde{x}_{t+1}^{in}, y_{t+1}^{rep}) \quad (34)$$

$$\tilde{\Delta}_{t+1}^{out} = (\mathcal{H}_{t+1}^{out}, \rho_{t+1}^{rep}, x_{t+1}^{in}, r_{t+1}, K_{t+1}, Q_{t+1}, R_{t+1}) \quad (35)$$

$$\tilde{\Pi}_{t+1} = \text{Prove}(pk, \theta, \mathcal{M}, \tilde{\Delta}_{t+1}^{in}, \tilde{\Delta}_{t+1}^{out}) \quad (36)$$

$$\Phi_{t+1} = \text{Verify}(vk, \tilde{\Pi}_{t+1}, \tilde{\Delta}_{t+1}^{in}, \tilde{\Delta}_{t+1}^{out}) = 1 \quad (37)$$

On the other hand, we can state that for ρ_{t+1}^{real} there also exists a system of proofs such that

$$\Delta_{t+1}^{in} = (\mathcal{H}_{t+1}^{in}, x_{t+1}^{in}, y_{t+1}^{real}) \quad (38)$$

$$\Delta_{t+1}^{out} = (\mathcal{H}_{t+1}^{out}, \rho_{t+1}^{real}, \tilde{x}_{t+1|t+1}, r_{t+1}, K_{t+1}, Q_{t+1}, R_{t+1}) \quad (39)$$

$$\Pi_{t+1} = \text{Prove}(pk, \theta, \mathcal{M}, \Delta_{t+1}^{in}, \Delta_{t+1}^{out}) \quad (40)$$

$$\Phi'_{t+1} = \text{Verify}(vk, \Pi_{t+1}, \Delta_{t+1}^{in}, \Delta_{t+1}^{out}) = 1 \quad (41)$$

We can clearly see that $\Delta_{t+1}^{out} \neq \tilde{\Delta}_{t+1}^{out}$, which implies that $\Pi_{t+1} \neq \tilde{\Pi}_{t+1}$. However, since both Δ_{t+1}^{out} and $\tilde{\Delta}_{t+1}^{out}$ are valid outputs of the pretrained model, we can further claim that $\Delta_{t+1}^{in} \neq \tilde{\Delta}_{t+1}^{in}$. Further analyzing $\Delta_{t+1}^{in}, \tilde{\Delta}_{t+1}^{in}$ we note that \tilde{y}_{t+1} is also probabilistically dissimilar to y_{t+1} . This means that the only viable possibility is that $(\mathcal{H}_{t+1}^{in}, x_{t+1}^{in}) \neq (\tilde{\mathcal{H}}_{t+1}^{in}, \tilde{x}_{t+1}^{in})$. However, this possibility contradicts our temporal consistency constraint thereby proving the intended statement.

(Case 2 Statistical consistency $\implies \Phi_{t+1} = 1$): Assume that $\Phi_{t+1} \neq 1$ where $\rho_{t+1}^{real} = \rho_{t+1}^{rep}$. We have a valid output Δ_{t+1}^{out} for an input Δ_{t+1}^{in} such that.

$$\Delta_{t+1}^{in} = (\mathcal{H}_{t+1}^{in}, x_{t+1}^{in}, y_{t+1}^{real}) \quad (42)$$

$$\Delta_{t+1}^{out} = (\mathcal{H}_{t+1}^{out}, \rho_{t+1}^{real}, x_{t+1}^{in}, r_{t+1}, K_{t+1}, Q_{t+1}, R_{t+1}) \quad (43)$$

$$\Phi_{t+1} = \text{Verify}(vk, \Pi_{t+1}, \Delta_{t+1}^{in}, \Delta_{t+1}^{out}) = 0 \quad (44)$$

Alternately, consider a case for a valid output $\tilde{\Delta}_{t+1}^{out}$ for an input $\tilde{\Delta}_{t+1}^{in}$ such that,

$$\tilde{\Delta}_{t+1}^{in} = (\tilde{\mathcal{H}}_{t+1}^{in}, \tilde{x}_{t+1}^{in}, y_{t+1}^{rep}) \quad (45)$$

$$\tilde{\Delta}_{t+1}^{out} = (\mathcal{H}_{t+1}^{out}, \rho_{t+1}^{rep}, x_{t+1}^{in}, r_{t+1}, K_{t+1}, Q_{t+1}, R_{t+1}) \quad (46)$$

$$\tilde{\Phi}_{t+1} = \text{Verify}(vk, \tilde{\Pi}_{t+1}, \tilde{\Delta}_{t+1}^{in}, \tilde{\Delta}_{t+1}^{out}) = 1 \quad (47)$$

Comparing $\tilde{\Phi}_{t+1}$ and Φ_{t+1} , we can conclusively say that $\tilde{\Delta}_{t+1}^{in} \neq \Delta_{t+1}^{in}$. Based on Lemma 1, we know that the underlying sensor measurement realizations $y_{t+1}^{real}, y_{t+1}^{rep}$ are probabilistically similar since statistical consistency is assumed. Since, $\tilde{\Delta}_{t+1}^{in}$ is a valid output of \mathcal{M} and $y_{t+1}^{real}, y_{t+1}^{rep}$ are probabilistically similar, we can say that the reason for $\tilde{\Phi}_{t+1} \neq \Phi_{t+1}$ is purely because of $(\mathcal{H}_{t+1}^{in}, x_{t+1}^{in}) \neq (\tilde{\mathcal{H}}_{t+1}^{in}, \tilde{x}_{t+1}^{in})$, which is a contradiction of our temporal consistency conditions establishing the soundness of the intended statement. \square

B.4. Proof of Theorem 4.3

Proof. For detection suppression, we assume that the compromised utility possesses an extractor \mathcal{E}^U that produces a valid proof Π_t which results in $\Phi_t = 1$ with an incorrect

witness $\mathcal{E}^A(\Delta_t^{in}, \Delta_t^{out}) \neq \Omega_t$, with a non-negligible probability. We consider \mathcal{E}^U producing proof Π_t which results in $\Phi_t = 1$ with an incorrect witness $\mathcal{E}^A(\Delta_t^{in}, \Delta_t^{out})$. Under the knowledge-soundness property of Halo2 [46], we can say

$$\Pr[\text{Verify}(vk_t, \Pi_t, \Delta_t^{in}, \Delta_t^{out}) = 1 \wedge ((\Delta_t^{in}, \Delta_t^{out}), \mathcal{E}^A(\Delta_t^{in}, \Delta_t^{out})) \notin \mathcal{R}_t] \leq \text{negl}(\lambda)$$

As a result, the knowledge-soundness property of Halo2 contradicts the assumption of detection suppression. We also know that the following claims hold $\forall t \geq t^{attack}$:

- C1** Key invariance ($vk_t = vk_{t+1}$ and $pk_t = pk_{t+1}$) is necessary for TC based on Theorem 4.1
- C2** Hash invariance $\mathcal{H}_{t+1}^{in} = \mathcal{H}_t^{out}$ and $\Phi_t = 1$ is a necessary and sufficient condition for TC based on Theorem 4.1.
- C3** TC for successive time steps under key invariance implies SC.

The infeasibility of detection suppression directly implies a violation of $\Phi_t = 1$ or of TC-SC relation \mathcal{R}_t . Either violation can be attributed to a violation of either **C1**, **C2** or **C3** applicable $\forall t \geq t^{attack}$.

Therefore, we can clearly establish that infeasibility of detection suppression is equivalent to violation of either the proof verification or the TC-SC relationship. \square

Appendix C. Additional Experimental Results

C.1. Proof Setup and Generation Times

The speedup relation used in Tables 4, 5 can be given as:

$$\text{speedup} = D \cdot \frac{(\text{average proving time for } D=1)}{(\text{average proving time for } D \neq 1)} \quad (48)$$

| Dataset | DVAL | CPU (%) | Memory (GB) |
|---------|------|-------------------|---------------|
| HAI | 16 | 1081.584(604.146) | 30.135(9.980) |
| ORNL-PS | 16 | 1081.584(604.146) | 30.135(9.980) |

TABLE 6: CPU and Memory Utilization (mean(std)) for Statistical consistency

The speedup computation is based on obtaining the ratio between the average time consumed for the entire set of D unrolled loop iterations when $D = 1$ and the corresponding values when $D \neq 1$. Since the time horizon appears in the numerator and denominator, they cancel each other resulting in Equation (48).

C.2. Detection Quality with varying PSF

In Figures 10 and 11, we depict the detection quality with respect to varying PSF values for distinct values of D . In this case we can observe that the lower PSF values usually exhibit greater volatility in detection, while higher PSF values correspond to a less volatile nature of the test statistic. Additionally, we also observe a slight increase in volatility with increasing D which is expected since the errors in residual computation compound for lower PSF values with

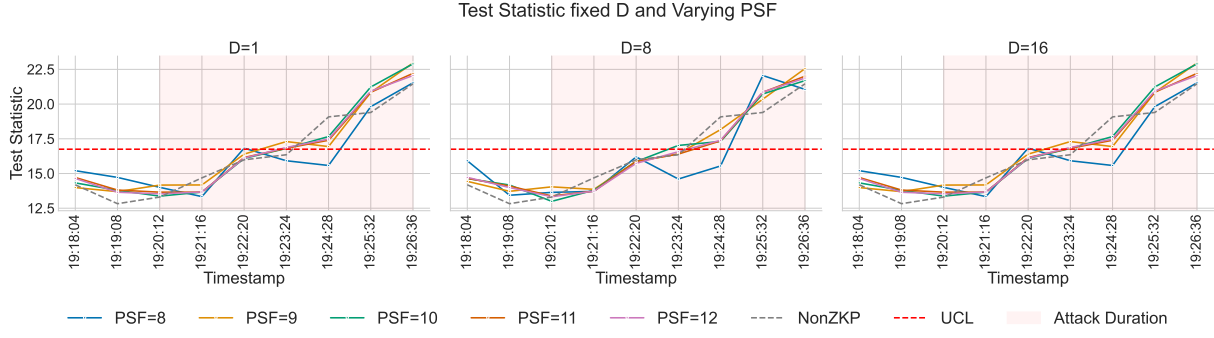


Figure 10: HAI Dataset: Detection Quality with varying PSF and fixed D

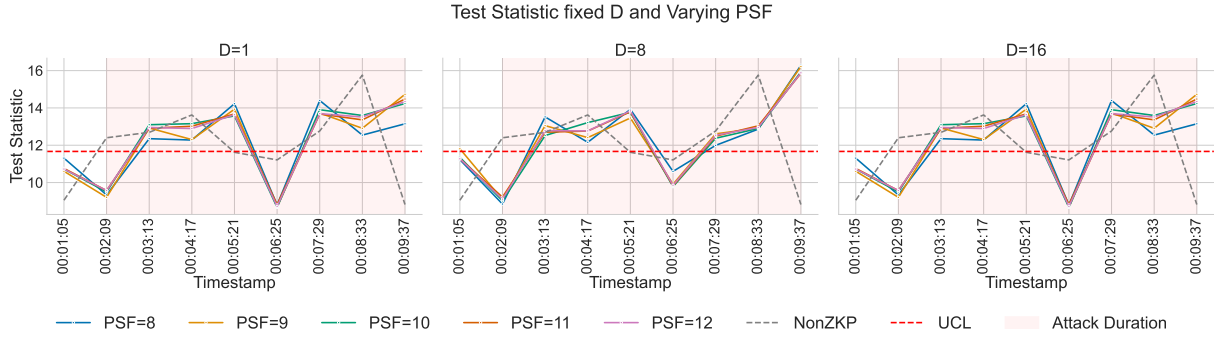


Figure 11: ORNL-PS Dataset: Detection Quality with varying PSF and fixed D

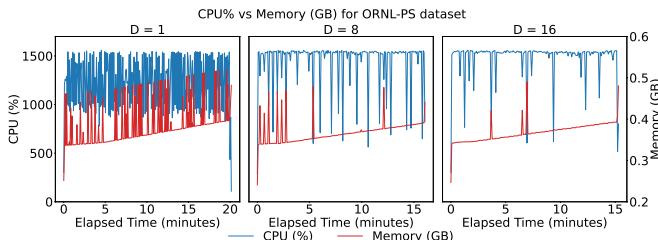


Figure 12: Witness Generation Performance with varying D for ORNL-PS dataset

| Setup Phase | Setup Time (s) | | | |
|---------------------|----------------|--------|--------|--------|
| | D=1 | D=4 | D=8 | D=16 |
| Model Export | 1.07 | 3.29 | 7.92 | 23.88 |
| Settings Generation | 0.74 | 3.73 | 9.80 | 29.20 |
| Circuit Compilation | 0.31 | 2.31 | 7.12 | 24.20 |
| Circuit Setup | 155.04 | 156.06 | 174.11 | 176.53 |

TABLE 7: HAI Setup Time Breakdown (in seconds)

| Setup Phase | Setup Time (s) | | | |
|---------------------|----------------|--------|--------|--------|
| | D=1 | D=4 | D=8 | D=16 |
| Model Export | 1.51 | 3.25 | 7.96 | 24.21 |
| Settings Generation | 0.74 | 3.53 | 9.55 | 28.99 |
| Circuit Compilation | 0.34 | 2.24 | 7.06 | 24.90 |
| Circuit Setup | 162.31 | 146.84 | 162.04 | 167.55 |

TABLE 8: ORNL-PS Setup Time Breakdown (in seconds)

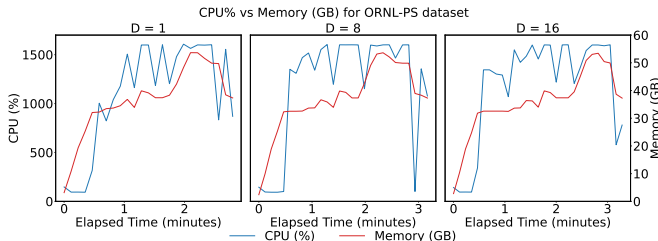


Figure 13: Prover Performance for Temporal Consistency with varying D for ORNL-PS dataset

higher D values. From these experiments, we can conclude that a higher PSF value might be more desirable for a lower D. However, a mid-range PSF value might also suffice for a higher D value. Regardless, the experiments establish the

robustness in detection quality of the zkSTAR framework.

C.3. Analysis of System Performance of ORNL-PS

Figures 12 and 13 present the system performance characterized by CPU utilization and memory consumption for ORNL-PS dataset for witness generation and proof generation mechanism. In Table 6, we provide the CPU utilization and memory consumption for the statistical consistency proofs for HAI and ORNL-PS datasets.

C.4. Analyses of Circuit Setup Costs

The mean setup times for HAI and ORNL-PS dataset has been provided in Tables 7 and 8 respectively for PSF values of 8, 10 and 12. These tables report zkSTAR times for model export, settings generation, circuit compilation, and circuit setup on the HAI and ORNL-PS datasets. The

TABLE 9: Verification times for HAI and ORNL-PS datasets (PSF=10).

| HAI | | | ORNL-PS | | |
|-----|------------|----------|---------|------------|----------|
| D | Type | Time (s) | D | Type | Time (s) |
| 1 | prediction | 1.22 | 1 | prediction | 1.26 |
| 8 | prediction | 1.34 | 8 | prediction | 1.40 |
| 16 | prediction | 1.09 | 16 | prediction | 1.31 |
| 16 | hypothesis | 1.24 | 16 | hypothesis | 1.46 |

results exhibit trends similar to Table 3, primarily reflecting circuit-size dependencies inherent to zk-SNARK setup.

C.5. Verification Times

Table 9 summarizes representative verification latencies for zkSTAR proofs under varying TC interval sizes of 1, 8 and 16 for prediction and hypothesis test components. Across all scenarios—including both normal and attack conditions—verification completed in approximately 1.0–1.5 s on commodity hardware, with all proofs passing successfully. These results confirm that zkSTAR’s zero-knowledge verification incurs minimal overhead and is practical for near-real-time regulatory audits.